A multi-stage methodology for wind park inter-array cabling: graph preparation, layout, and sizing

Bernardo Castro Valerio[1,2], Pieter M.O.Gebraad[1], Marc Cheah-Mane[2], Vinicius A. Lacerda[2], and Oriol Gomis-Bellmunt[2]

[1]Youwind, Barcelona, Spain
[2]Centre d'Innovació Tecnològica en Convertidors Estàtics i Accionaments, Departament d'Enginyeria Elèctrica, Universitat Politècnica de Catalunya, Barcelona, Spain

Correspondence: Bernardo Castro Valerio (bcv@youwindrenewables.com)

Abstract.

Inter-array grid optimisation plays a critical role in the technical and economic performance of wind parks and is typically divided into two primary tasks: layout length minimisation and conductor size selection. This work proposes the consideration of three primary tasks, beginning with graph preparation to account for terrain profiles, soft and hard exclusion zones, and export cables. Once a graph with viable connection pathways is established, a routing mixed-integer linear formulation for radial arrays, subject to crossing constraints and a maximum number of turbines per string, is presented. This formulation can be adapted to user requirements to include a minimum number of turbines per string, as well as a methodology to determine the minimum number of substation connections required under irregular turbine distributions arising from terrain constraints. Conductor size selection is addressed through a linear approximation of the power flow, enabling the limitation of the number of conductor types used within the system. Routing and conductor size selection may be combined within an integrated approach or implemented as a sequential algorithm to explore trade-offs between trenching and cabling costs. The proposed approaches are evaluated using current turbine ratings and the layouts of existing onshore and offshore projects. The integrated formulation generally achieves lower total costs, while the sequential approach offers greater modelling flexibility for constrained routing problems. The results further demonstrate that layouts with minimum trench length do not necessarily minimise total investment cost, since limiting the number of conductor types may exclude larger conductor capacities, thereby changing the feasible routing configurations and the conductor types ultimately selected within the system.

1 Introduction

Wind energy has become a central component of the global energy transition. In wind park design, once turbine locations have been determined through wind resource and wake optimisation, attention shifts to the inter-array cable system, which interconnects turbines and transmits power to substations. The configuration of this electrical collection network is shaped by routing complexity arising from terrain conditions, spatial constraints, and installation limitations. Optimising this configuration is highly relevant for cost-effectiveness; for example, in bottom-fixed offshore wind farms, inter-array cables may account for up to approximately 8-9% of the levelised cost of energy (LCoE) (Serrano González et al., 2014; BGV Associates, 2025).

The design of the cable array constitutes a critical aspect of the overall wind park configuration. This process may be divided into two primary tasks: first, collector system optimisation to minimise cable lengths; and second, conductor size selection (CSS). In the collector system optimisation phase, multiple topologies have been implemented in practice, including radial, radial plus star, radial plus star with splices, single loop, and others (Pérez-Rúa and Cutululis, 2019). To address collector system optimisation, various approaches have been employed, including graph-based methods derived from the minimum spanning tree (MST) and travelling salesman problem (TSP) formulations (Dutta and Overbye, 2012; Wei et al., 2017), ant colony optimisation (Taylor et al., 2023), mixed-integer linear programming (MILP) (Fischetti and Pisinger, 2018a, b; Pillai et al., 2015; Pérez-Rúa et al., 2020; Ulku and Alabas-Uslu, 2020; Souza de Alencar et al., 2025), and heuristic approaches (Cazzaro et al., 2020; El Mokhi and Addaim, 2020; Sedighi et al., 2018; Gong et al., 2018), including genetic algorithms (Moon et al., 2014; Wei et al., 2017; Smail et al., 2018) and particle swarm optimisation (Hou et al., 2016). In this context, a balanced configuration refers to limiting disparities in the number of turbines connected per substation and per string, thereby resulting in advantages in installation planning and transformer specification, as discussed in (Cazzaro and Pisinger, 2022).

The collector system optimisation model in the work of Fischetti and Pisinger (2018a) formulates a MILP problem for cable routing that incorporates exclusion zones, but considers only straight-line connections, which limits layout flexibility. Similarly, the work of Ulku and Alabas-Uslu (2020) restricts the number of node connections, while Pillai et al. (2015) introduces an iterative MILP to address crossing constraints. None of the approaches in Wędzik et al. (2016); Fischetti and Pisinger (2018a); Ulku and Alabas-Uslu (2020); Pillai et al. (2015); Pérez-Rúa et al. (2020) enforce radial arrays, as they permit bifurcations at turbine nodes. The work of Fischetti and Pisinger (2018b) includes a string structure but relies on a directed graph, which imposes directional flow towards substations and limits flexibility. Reference Souza de Alencar et al. (2025) presents a MILP with undirected graphs and radial array, inherently addressing line-of-sight and cable crossings; however, it lacks the capacity to model clearance constraints from fixed structures. In both Fischetti and Pisinger (2018b); Souza de Alencar et al. (2025), lengths are calculated using purely Euclidean 2D distances. Reference Gong et al. (2018) applies a geodesic algorithm on a 3D seabed, effective for ring structures simplified into strings by removing central links, but it omits GIS constraints.

The second task involves appropriately sizing the conductor to balance power flow requirements with investment costs. This can be achieved either through static rated sizing, which assumes a continuous current over time, or through a dynamic load cycle profile, which accounts for the variability of power production (Pérez-Rúa and Cutululis, 2019). To address the CSS problem, studies have employed genetic algorithms (Smail et al., 2018; Rentschler et al., 2019), modified bat algorithms (Qi et al., 2019), and MILP formulations (Wędzik et al., 2016; Chen et al., 2016; Fischetti and Pisinger, 2018a; Pérez-Rúa et al., 2020).

In terms of integrated layout and CSS solutions, Wędzik et al. (2016) combines a simple layout generation with a CSS constrained to a single substation per graph. In Pérez-Rúa et al. (2020), an integrated layout algorithm is proposed that can adapt to multiple substations and limit static crossings; however, when considering CSS, the method does not limit the number of permitted conductors. Due to the cost associated with cable-laying vessel operations, the number of different conductor diameters used in offshore wind farms design is typically limited.

Regarding a pure CSS problem, Sedighi et al. (2018) employs a harmony search algorithm for partial cable sizing, whereby each branch along a route is assigned a conductor based on the ampacity of the final segment before it joins another route or connects to the substation. The study considers branches originating from bifurcation points; thus, in radial arrays the same conductor type is assigned to all sections of a string.

This work builds on Valerio et al. (2026b), which presents the graph preparation methodology and the mixed-integer linear formulation for routing of inter-array connections. In addition, this paper presents two methods for joint routing and conductor size optimisation. The first is an integrated approach that incorporates conductor size selection directly into the routing algorithm. The second is a sequential solution that iterates between routing and CSS, addressing a more constrained problem. Following Hou et al. (2019); Kallinger et al. (2023) and the revised literature, an algorithm designed to address the inter array cabling of wind turbines should satisfy the following criteria:

C1, Consider nonhomogeneous terrain conditions

C2. Avoid cable crossings in the layout.

C3. Ensure that the current in each cable under full load conditions does not exceed its rated capacity.

C4. For a radial array, no bifurcations are allowed in turbine nodes.

C5. Limit the number of different conductor type sections.

C6. Aim to reduce computational cost.

To address these criteria, the main contributions of this work are as follows:

- A graph construction methodology that incorporates three-dimensional terrain, inclination constraints, and both hard and soft exclusion zones into the candidate edge generation process.
- A reduced MILP formulation for inter-array routing using a single binary variable per arc, thereby decreasing the number of decision variables relative to standard formulations.
- A joint treatment of routing and conductor size selection, allowing CSS to influence layout decisions rather than being treated as post-processing.
- The development and comparison of integrated and sequential approaches for joint routing and CSS, highlighting trade-offs between solution quality and computational complexity.

The final solution includes a graph preparation phase that incorporates exclusion zones and elevation into the identification of connections process (Section 2). The routing algorithm is presented in Section 3.1, with additional modelling options described in Section 3.2, including constraints on the minimum number of turbines per string, the determination of substation connections, and unbalanced substation capacities. A stand-alone CSS formulation is introduced in Section 4. Joint routing and conductor size optimisation are then addressed through an integrated formulation (Section 5.1) and a sequential algorithm (Section 5.2). The approaches are evaluated in Section 6, with the results discussed in Section 7.

2 Graph preparation

Graphs are commonly constructed using geometric two-dimensional distances between turbines. However, the quality of the optimisation strongly depends on the granularity and realism of the input data. To make the cable routing problem more accurate, it is necessary to incorporate additional spatial constraints, including bathymetry, inclination, and exclusion zones. Fig. 1 illustrates the procedure for generating viable graph edges. The process integrates bathymetric or elevation data, turbine and substation locations, and spatial constraints such as inclination limits, clearance constraints, and exclusion zones. The methodology consists of the following steps (a–f), shown sequentially in the figure.

(a) The turbine and substation coordinates are transformed from the geographic coordinate system (latitude and longitude) to Cartesian coordinates, with the origin positioned at the first substation.

(b) A line-of-sight analysis is conducted between turbines and substations, with intermediate points added along unobstructed paths. Line-of-sight is defined as a direct path that remains within the development area, avoids exclusion zones and export cable crossings, and maintains a specified clearance distance from intermediate turbines or substations. The development area is then partitioned into triangular regions using Delaunay triangulation Virtanen et al. (2020), with vertices defined by points from the development boundary, exclusion zones, turbines, and substations. Candidate line-of-sight connections are discretised by inserting linearly interpolated points at evenly spaced intervals along each unobstructed segment, with the number of samples increasing proportionally to segment length, while each Delaunay triangle is populated with additional vertices generated from a regular grid of points defined in barycentric coordinates, with a fixed number of subdivisions per edge, including both edge and interior points. Together, these two processes produce a densified set of points, improving routing flexibility by relaxing the constraint of strictly direct paths.

(c) A predefined bathymetric measurement grid is overlaid to encompass all densified points; in this study, data from (GEBCO Bathymetric Compilation Group, 2025) are employed. Each point is assigned a z-coordinate, interpolated from the nearest available measurements.

(d) The densified points are interconnected using the line-of-sight chains, Delaunay triangulation, and additional diagonal connections, ensuring each point is linked to its surrounding neighbours. For each segment, the three-dimensional Euclidean distance is computed. Segments that exceed a specified inclination threshold or intersect an export cable route are excluded from further consideration.

Exclusion zones are then analysed. These may include, but are not limited to, protected natural areas, fishing zones, or specific soil types. When sufficient information is available, each exclusion zone is classified as either a hard or soft exclusion. For hard-exclusion zones, densified nodes located within them, as well as those outside the designated development area, are removed from the dataset, thereby also removing the segments connected to them. Two distinct quantities are associated with each remaining graph segment:

(i) an *edge weight*, used for routing and trenching cost estimation, and (ii) an *edge length*, used for cable cost estimation.

Initially, the edge weight is equal to the edge length. However, for segments crossing soft-exclusion zones, a penalty factor is applied to the edge weight, discouraging their use while still permitting routing through such areas when necessary. The geometric length remains unchanged.

The penalty factor is defined based on engineering judgement and site-specific conditions, such as seabed soil characteristics, and is ultimately translated into an increased CAPEX contribution within the MILP optimisation. For example, in Fig. 1(d) in red, a shipwreck is shown as a hard-exclusion zone, while an orange area represents a soft-exclusion that increases edge weights by 50%.

(e) Dijkstra's algorithm (Hagberg et al., 2008) is used to construct inter-turbine paths from the previously densified segments. The adjacency structure between turbines is defined using a Delaunay triangulation of the turbine positions, augmented with cross-diagonal connections between opposite vertices of adjacent triangles. Each resulting shortest path, consisting of multiple densified segments, is represented as a single candidate edge in the optimisation graph.

To construct turbine-substation candidate edges, subgraphs are generated for each turbine, excluding all other turbines and any points within a defined protection radius. Turbine-substation paths are then obtained using the A* algorithm (Hagberg et al., 2008), with the substation specified as the starting node and the turbine as the target. Each resulting route is represented as a single candidate edge.

For each candidate edge, both the edge weight and edge length are computed by summing the corresponding quantities of its component segments. Pairs of intersecting or overlapping turbine-turbine edges (a, b) are identified and recorded. For turbine-substation edges, intersections are identified only with edges that do not share the same substation; crossings between edges connected to the same substation are excluded from comparison.

For offshore facilities, an additional vertical distance from the seabed to sea level is added at each endpoint to the edge length, representing the cable reaching the turbine or substation along the sub-sea foundation. This vertical component does not modify the edge weight, as trenching is only associated with seabed routing.

(f) Finally, the inter-turbine and turbine-substation edges are merged into a single undirected weighted graph, representing all candidate interconnections within the system.

3 Collector system routing

The second stage of the array optimisation process involves taking the undirected graph of feasible edges and selecting a configuration that minimises the total connection weight required to link all turbines to the substations. To achieve this, a MILP is formulated. The associated constraints are designed to enforce a radial array topology, limit the maximum number of turbines connected per string, and prevent edge crossings. A radial array is defined as a set of cable strings connecting turbines to substations without cycles. Each turbine lies on a simple path to a substation and may connect to at most two neighbouring nodes.

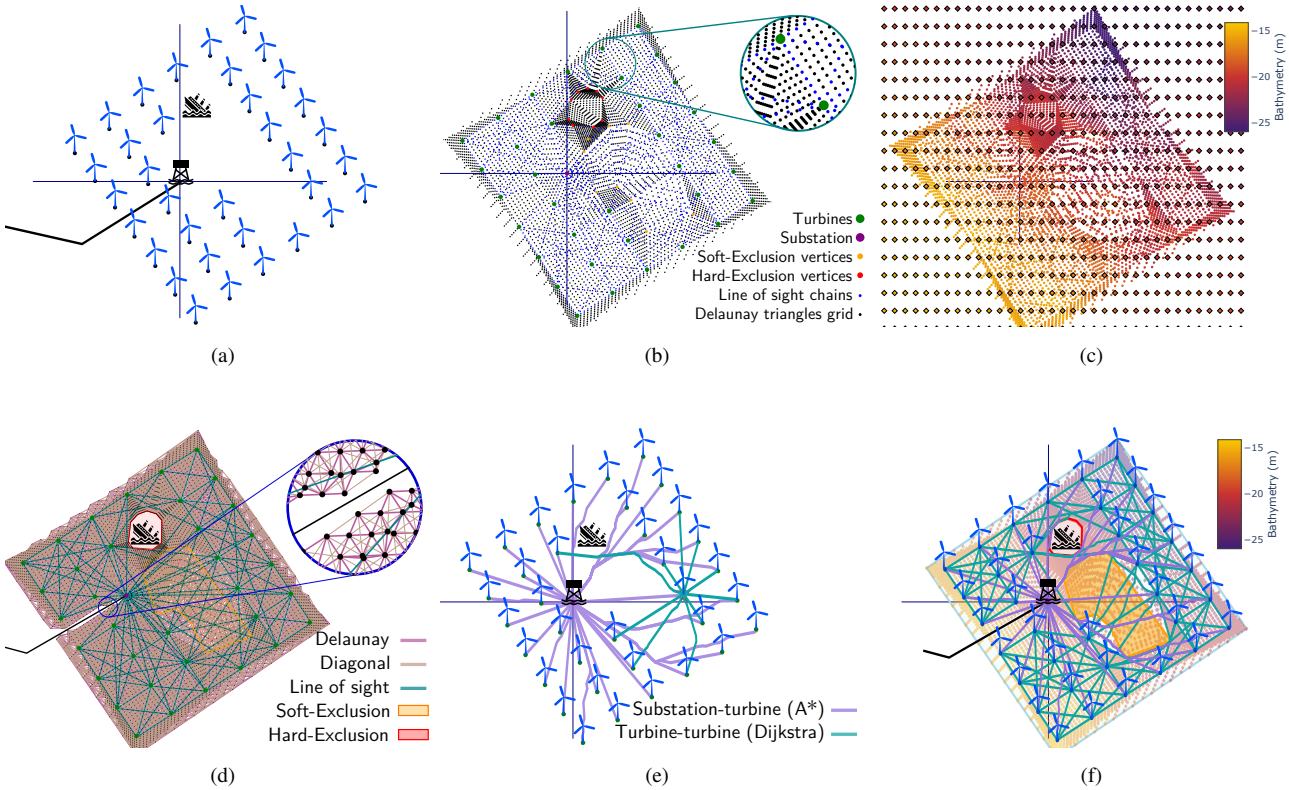

Figure 1. Graph edge preparation: (a) Turbine group, (b) Densified grid, (c) Elevation overlay, (d) Densified graph, (e)Inter-paths, (f) Final graph.

3.1 Core formulation

The graph nodes ($\mathcal{N}_{ac}$) are initially partitioned into two sets: turbine nodes $\mathcal{N}_t \subseteq \mathcal{N}_{ac}$ and substation nodes $\mathcal{N}_s \subseteq \mathcal{N}_{ac}$, such that $\mathcal{N}_{ac} = \mathcal{N}_t \cup \mathcal{N}_s$. To maintain power flow tracking within the system, each turbine node injects one unit of power, modelled as a fixed parameter such that $p_i = 1$ for all $i \in \mathcal{N}_t$.

For substation nodes, the net injection is modelled as an integer decision variable representing representing power withdrawal, such that $p_i \in \mathbb{Z}_{\leq 0}$ for all $i \in \mathcal{N}_s$.

Power balance is enforced by requiring that the total substation withdrawal matches the total turbine injection:

$$\sum_{i \in \mathcal{N}_s} p_i = -|\mathcal{N}_t|. \tag{1}$$

Units of power are transferred through each edge and an integer variable $f_a \in \mathbb{Z}$ is associated with each candidate edge $a \in \mathcal{E}$, representing the number of turbine units transmitted between nodes i and k. Although the graph is undirected, each edge $a = (i, k)$ is assigned an arbitrary reference orientation for flow accounting purposes. A negative value of f_a therefore

indicates flow opposite to the chosen orientation. The following constraint ensures that the power generated by all turbines is transmitted through the grid, and that no turbine remains unconnected:

$$p_i = \sum_{\substack{a=(i,k)\in\mathcal{E} \\ k\in\mathcal{N}_{ac},\, k\neq i}} f_a \qquad \forall i \in \mathcal{N}_{ac}. \tag{2}$$

To determine whether an edge is selected within the system, a binary variable $\xi_a \in \{0,1\}$ is assigned to each candidate edge, indicating whether the corresponding edge is activated. To guide the optimisation towards selecting an appropriate number of edges, the following constraint is introduced:

$$\sum_{a\in\mathcal{E}} \xi_a = |\mathcal{N}_t|. \tag{3}$$

This constraint states that the minimum number of edges required to interconnect all nodes in a single graph is one less than the number of nodes. Accordingly, the number of edges necessary to connect all turbines to a given number of disjoint substations can be determined, resulting in the formation of separate graphs within the wind farm structure.

Furthermore, the binary variable enables the restriction of crossing pair activations, ensuring that at most one edge from each crossing pair is active. Crossing pairs are defined by the set $\mathcal{X}$ which denotes the set of unordered edge pairs (a,b) such that edges a and b geometrically intersect, as constrained by:

$$\xi_a + \xi_b \leq 1 \qquad \forall (a,b) \in \mathcal{X}. \tag{4}$$

To limit the maximum number of turbines connected via a single string, the power flow on each edge is constrained such that

$$-\xi_a \cdot \mathfrak{M} \leq f_a \leq \xi_a \cdot \mathfrak{M}. \tag{5}$$

Here, $\mathfrak{M}$ is a parameter that represents the maximum allowable integer power flow per edge, equivalent to the maximum number of turbines per string, and ξ_a ensures that no power is permitted through inactive edges. To regulate the number of permissible connections at each turbine node, the following constraint is imposed,limiting the number of active edges connected to each turbine node.

$$1 \leq \sum_{a\in\mathcal{E}_i} \xi_a \leq 2 \qquad \forall i \in \mathcal{N}_t. \tag{6}$$

This is achieved by summing the binary activation values over the subset $\mathcal{E}_i \subset \mathcal{E}$ of edges connected to node i. In radial arrays, this threshold is set to two for turbine nodes, ensuring that each turbine is connected to at most two active edges

and thereby preventing bifurcations. Relaxing this constraint permits bifurcations and enables radial-star configurations when required.

A key consideration in the design of array systems is the number of permissible string connections to a substation. This is enforced by the following constraints:

$$\mathfrak{s}_s \leq \sum_{a \in \mathcal{E}_i} \xi_a \leq \mathfrak{S}_s \qquad \forall i \in \mathcal{N}_s, \tag{7a}$$

$$\mathfrak{s}_s = \left\lceil \frac{|\mathcal{N}_t|}{|\mathcal{N}_s| \cdot \mathfrak{M}} \right\rceil. \tag{7b}$$

Here, $\mathfrak{S}_s$ denotes the maximum number of string connections permitted at each substation node $i \in \mathcal{N}_s$ and is treated as a fixed integer within each MILP solve. To reduce the search space, the minimum number of string connections per substation, $\mathfrak{s}_s$, determines the distribution according to the maximum number of turbines permitted in each string.

The objective of the optimisation is to minimise the total weight of all active edges, defined as

$$\min \left[\sum_{a \in \mathcal{E}} \xi_a \cdot \mathcal{W}_a \right]. \tag{8}$$

Here, $\mathcal{W}_a$ denotes the pre-computed weight of edge a obtained during the graph preparation step (e).

3.2 Additional design constraints

To improve the practicality and balance of the solutions produced by the core MILP formulation, additional modelling strategies are introduced. These refinements aim to guide the optimisation process towards layouts that are not only feasible but also well-structured in terms of string distribution and substation connectivity.

3.2.1 Minimum turbines per string

Another sub-strategy to balance strings involves enforcing a minimum number of turbines per string. To achieve this, we define the subset $\mathcal{E}_s \subseteq \mathcal{E}$, comprising edges that connect turbines to a substation, drawn from the set of all permissible graph edges. Certain considerations must be taken into account for any edge $a \in \mathcal{E}_s$. Firstly, for turbine-substation connections, the edge is treated as directed from the turbine to the substation, denoted as $a : (i, k)$ with $i \in \mathcal{N}_t$ and $k \in \mathcal{N}_s$. This convention preserves the logic of Eq. (2), enabling the introduction of the following inequality constraint:

$$\xi_a \cdot \mathfrak{m} \leq f_a \leq \xi_a \cdot \mathfrak{M} \qquad \forall a \in \mathcal{E}_s. \tag{9}$$

Here, $\mathfrak{m}$ denotes the minimum turbine unit flow per string. To balance the number of turbines per string based on $\mathfrak{M}$, the minimum number of connections to the substations is determined from Eq. (7). Following this logic, $\mathfrak{m}$ can be calculated as

$$\mathfrak{m} = \left\lfloor \frac{|\mathcal{N}_t|}{\mathfrak{s}_s \cdot |\mathcal{N}_s|} \right\rfloor . \tag{10}$$

For example, in an array group comprising 50 turbines, and assuming a maximum string capacity of seven, the minimum number of connections to the substation is eight, whereas the minimum number of turbines per string is six.

3.2.2 Determination of Substation Connections

Due to connectivity and crossing constraints, determining an appropriate value for the number of substation connections is not always straightforward. If the range between $\mathfrak{s}_s$ and $\mathfrak{S}_s$ is too large, the algorithm may produce numerous very short strings, resulting in an unbalanced electrical grid. To mitigate this, a simple iterative algorithm is employed. It determines the minimum feasible value of the maximum number of substation connections, $\mathfrak{S}_s$, required to ensure full turbine connectivity.

The algorithm begins by computing the ceiling of the division of the number of turbines by the product of the number of substations and the maximum number of turbines per string, as shown in Eq. (7b), and setting $\mathfrak{S}_s = \mathfrak{s}_s$. This estimate aims to distribute the strings evenly across substations. If the resulting layout is infeasible, the value of $\mathfrak{S}_s$ is incrementally increased by one until a feasible solution is found.

As the required connections to the substation increase at each iteration, if the determination of the number of substation connections is combined with the minimum number of turbines per string, Eq. (10) must be modified to use the maximum bound, such that

$$\mathfrak{m} = \left\lfloor \frac{|\mathcal{N}_t|}{\mathfrak{S}_s \cdot |\mathcal{N}_s|} \right\rfloor . \tag{11}$$

3.2.3 Unbalanced Substation Capacity

In certain projects, circumstances may necessitate the installation of substations with differing capacities, such as in spatially separated development areas. In such cases, constraint Eq. (1) must be further specified as follows:

$$p_i \geq -s_i^{\max} \qquad \forall i \in \mathcal{N}_s, \tag{12a}$$

$$\sum_{i \in \mathcal{N}_s} s_i^{\max} \geq |\mathcal{N}_t|. \tag{12b}$$

Here, each substation is limited by a maximum per-unit capacity, denoted by $s_i^{\max}$. The inequality is formulated such that the flow is greater than or equal to the limit because p_i represents the outgoing flow of the system and is assumed to take negative values. To accommodate differing capacities, it is required that the total installed capacity across all substations equals or exceeds the number of turbines, as specified in Eq. (12b), which acts as a consistency condition on the user-defined input parameters rather than a constraint involving optimisation variables, since substation capacities are fixed inputs and not subject to optimisation.

4 Conductor size selection

The conductor size selection (CSS) problem determines the appropriate diameter for each cable section from a restricted set of available park conductor types. For every connection between two nodes, a cable type ι must be selected from the mutually exclusive set $\mathcal{I}$, allowing only one conductor type per connection.

In this section, the CSS problem is formulated assuming that the network routing has already been determined. Let $\mathcal{A} \subseteq \mathcal{E}$ denote the subset of active edges selected during the routing stage, such that $\xi_a = 1$ for all $a \in \mathcal{A}$. Under this formulation, the optimisation assigns a conductor type to each active connection such that the power flow requirements are satisfied while minimising the total conductor investment cost. Each conductor type $\iota \in \mathcal{I}$ is characterised by a conductor cost per unit length ψ_ι. Accordingly, the objective function is defined as:

$$\min \left[\sum_{a \in \mathcal{A}} \sum_{\iota \in \mathcal{I}} \xi_{a,\iota} \cdot L_a \cdot \psi_\iota \right]. \tag{13}$$

Here, $\xi_{a,\iota}$ is a binary variable indicating whether conductor type ι is assigned to edge a, and L_a denotes the pre-computed length of edge a obtained during the graph preparation step (e).

4.1 Non-Linear CSS

One possible formulation for cable size selection employs a non-linear model of AC power flow (ACOPF). This formulation considers the voltage magnitude V and angle θ at each node, and calculates the active P and reactive Q power flowing in each branch based on the branch admittance representation derived from $Y = G + jB$. The apparent power S_{ik} from node i to node k is then defined as

$$S_{ik} = P_{ik} + \mathrm{j}Q_{ik}, \tag{14a}$$

$$P_{ik} = |V_i|^2 G_{ff} + |V_i||V_k| \left[G_{ft} \cos(\theta_i - \theta_k) + B_{ft} \sin(\theta_i - \theta_k) \right], \tag{14b}$$

$$Q_{ik} = -|V_i|^2 B_{ff} + |V_i||V_k| \left[G_{ft} \sin(\theta_i - \theta_k) - B_{ft} \cos(\theta_i - \theta_k) \right]. \tag{14c}$$

Each node $i \in \mathcal{N}_{ac}$ is assumed to correspond to either a turbine or a substation, such that at most one of P_{t_i} or P_{s_i} is non-zero. Accordingly, the nodal power balance is given by

$$\gamma_{t_i} P_{t_i} - P_{s_i} = \sum_{\substack{k \in \mathcal{N}_{ac} \\ k \neq i}} P_{a_{\text{ik-eq}}} \qquad \forall i \in \mathcal{N}_{ac}, \tag{15a}$$

$$Q_{t_i} - Q_{s_i} = \sum_{\substack{k \in \mathcal{N}_{ac} \\ k \neq i}} Q_{a_{\text{ik-eq}}} \qquad \forall i \in \mathcal{N}_{ac}. \tag{15b}$$

Here, variables P_{t_i} and Q_{t_i} denote the active and reactive power generated at node i by a connected turbine, while P_{s_i} and Q_{s_i} represent the corresponding substation consumption. The term $\gamma_{t_i} P_{t_i}$ represents curtailed generation, where $\gamma_t = 1 - \text{curtailment}_{pu}$.

This allows the consideration of the trade-off between system losses and cable investment costs. Non-linear modelling captures the complete π model of cables, including inductance and, crucially for submarine cables, capacitance, which can increase reactive power and thereby lead to additional losses. The formulation of a non-linear CSS power flow is presented in (Valerio et al., 2026a), where each array section a includes multiple $Y_{\text{bus-branch}}$ elements corresponding to the various conductor types that may connect the node pair, as illustrated in Fig. 2.

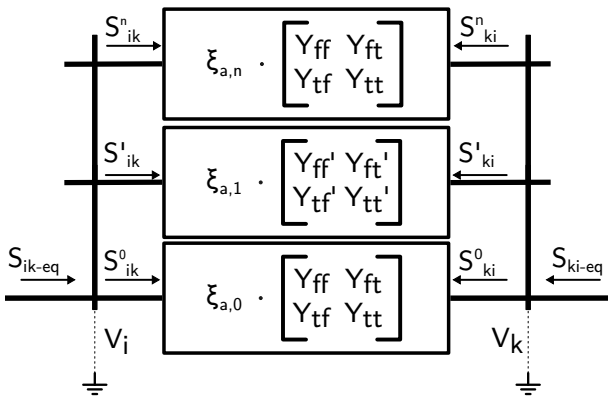

Figure 2. AC power as a function of the $\xi_{a,\iota}$ factor

The use of equivalent bus admittance matrices establishes a relationship in which the power at each end of the equivalent branch is determined by multiple binary factors $\xi_{a,\iota} \in \{0,1\}$, which relate the apparent power flow associated with each conductor type, $S_{a,\iota}$, to the equivalent branch flows $S_{a_{\text{ik}}\text{-eq}}$ and $S_{a_{\text{ki}}\text{-eq}}$, such that

$$S_{a_{\text{ik}}\text{-eq}} = \sum_{\iota \in \mathcal{I}} \left(\xi_{a,\iota} \cdot S_{a,\iota_{\text{ik}}} \right), \tag{16a}$$

$$S_{a_{\text{ki}}\text{-eq}} = \sum_{\iota \in \mathcal{I}} \left(\xi_{a,\iota} \cdot S_{a,\iota_{\text{ki}}} \right). \tag{16b}$$

Here, $S_{a,\iota_{ik}}$ denotes the apparent power flow associated with conductor type ι on branch $a = (i,k)$, directed from node i to node k, where $\xi_{a,\iota}$ is indexed by both the branch position a and the conductor type $\iota \in \mathcal{I}$. The referenced paper presents a non-linear approach that considers internal system losses, allowing for the intentional over-sizing of conductor sections to reduce losses. These losses are incorporated into the main CSS objective within a multi-objective framework as follows:

$$\min \left[\frac{1-(1+r)^{-y}}{r} \cdot H_y \cdot \rho \cdot \left(\sum_{i \in \mathcal{N}_t} P_{t_i} - \sum_{i \in \mathcal{N}_s} P_{s_i} \right) \right]. \tag{17}$$

Here, the losses are calculated as the total power extracted by the substations, $\sum_{i\in\mathcal{N}_s} P_{s_i}$, minus the total power injected by the turbines, $\sum_{i\in\mathcal{N}_t} \gamma_{t_i} P_{t_i}$, in the array system. The economic parameter H_y denotes the full-load hours of system operation over y years, while ρ denotes the electricity cost, for example based on an assumed LCoE. The discount rate r enables a net present value (NPV) comparison with conductor investment costs. Both individual objectives are combined into a multi-objective function using a weighting parameter $\alpha \in \mathbb{R}_{\geq 0}$, which determines the relative importance of the loss-related term,

$$\min\left[(13) + \alpha(17)\right]. \tag{18}$$

4.2 Linear CSS

While non-linear modelling provides the most comprehensive representation of losses and power flow, it can be computationally intensive. If efficiency is a priority, a strategy based on a linear simplification of power flows, commonly referred to as the DCOPF approximation, can be adopted. This subsection presents the corresponding equality and inequality constraints associated with this formulation.

4.2.1 Equality constraints

The linear power flow approximation assumes that voltage magnitudes remain constant and close to one per unit at all nodes, while the voltage angle differences between connected nodes are small. Under these assumptions, the AC power flow equation simplifies to

$$P_{a,\iota_{\text{ik}}} = -\Im\{Y_{\text{bus}_{ik}}\} \cdot (\theta_i - \theta_k). \tag{19}$$

Here, the active power flow is computed using the negative imaginary part of the corresponding Y_{bus} entry for each conductor.

To establish the real power balance at each node, the equivalent formulation equates the net power injection from turbines (t) and substations (s) to the corresponding power flows within the system:

$$\gamma_t P_{t_i} - P_{s_i} = \sum_{\substack{k\in\mathcal{N}_{ac}\\ k\neq i}} P_{a_{\text{ik-eq}}} \qquad \forall i \in \mathcal{N}_{ac}. \tag{20}$$

Following Eq. (16), the equivalent real power flow across each connection is described by Eq. (21a). However, to avoid introducing a quadratic constraint resulting from the product of binary and continuous variables, McCormick envelopes are applied using auxiliary variables $z_{a,\iota}$:

$$P_{a_{\text{ik-eq}}} = \sum_{\iota\in\mathcal{I}} \left(\xi_{a,\iota} \cdot P_{a,\iota_{\text{ik}}}\right), \tag{21a}$$

$$P_{a_{\text{ik-eq}}} = \sum_{\iota\in\mathcal{I}} z_{a,\iota}. \tag{21b}$$

To support this linearisation, a big-M parameter is introduced to relax specific constraints involving binary variables. In this study, it is defined in Eq. (22), where M_a represents the maximum allowable power for any conductor type in branch a, scaled by a security factor κ. The value of κ is set to 1.1. This parameter acts as an upper bound, effectively deactivating flow constraints when the corresponding binary variable indicates that the conductor is not selected:

$$M_a = \kappa \cdot \max\left[P_{a,\iota}^{\max} \, \forall \iota \in \mathcal{I}\right]. \tag{22}$$

4.2.2 Inequality Constraints

The McCormick envelopes are constructed such that Eq. (23a) and Eq. (23b) enforce an equality between z and P when ξ is active. When ξ is inactive, both constraints are relaxed by the maximum power M_a, ensuring feasibility regardless of flow. In addition, Eq. (23c) and Eq. (23d) define the bounds on z: when ξ is active, these bounds correspond to the maximum power permitted by the selected conductor; when inactive, z is constrained to zero.

$$z_{a,\iota_{\text{ik}}} \leq P_{a,\iota_{\text{ik}}} + (1-\xi_{a,\iota}) \cdot 2M_a, \tag{23a}$$

$$z_{a,\iota_{\text{ik}}} \geq P_{a,\iota_{\text{ik}}} - (1-\xi_{a,\iota}) \cdot 2M_a, \tag{23b}$$

$$z_{a,\iota_{\text{ik}}} \leq \xi_{a,\iota} \cdot P_{a,\iota}^{max}, \tag{23c}$$

$$z_{a,\iota_{\text{ik}}} \geq -\xi_{a,\iota} \cdot P_{a,\iota}^{max}. \tag{23d}$$

Thermal limits for each branch are enforced by bounding the flow $P_{a,\iota_{\text{ik}}}$ to comply with criterion C3. The following constraints implement this limitation, with activation governed by $\xi_{a,\iota}$. When inactive, the constraints are relaxed using the big-M formulation:

$$P_{a,\iota_{\text{ik}}} \leq \quad P_{a,\iota}^{max} \cdot \xi_{a,\iota} + M_a \cdot (1-\xi_{a,\iota}) \qquad \forall a \in \mathcal{A}, \, \forall \iota \in \mathcal{I}, \tag{24a}$$

$$P_{a,\iota_{\text{ik}}} \geq -P_{a,\iota}^{max} \cdot \xi_{a,\iota} - M_a \cdot (1-\xi_{a,\iota}) \qquad \forall a \in \mathcal{A}, \, \forall \iota \in \mathcal{I}. \tag{24b}$$

For the CSS selection, one conductor must be chosen for each section, as enforced by the following constraint:

$$\sum_{\iota \in \mathcal{I}} \xi_{a,\iota} = 1 \qquad \forall a \in \mathcal{A}. \tag{25}$$

To track which conductor types are used in the overall system and comply with criteria C5, the binary indicator $\nu_\iota \in \{0,1\}$ is introduced. This indicator identifies whether conductor type ι is active within the system. The following constraints ensure that ν_ι is assigned consistently. In particular, Eq. (26a) enforces that if one or more $\xi_{a,\iota}$ values are active across any connection a, then ν_ι must be set to one, whereas Eq. (26b) ensures that if no $\xi_{a,\iota}$ variables are active for a given ι, then ν_ι must be zero.

$$\sum_{a\in\mathcal{A}} \xi_{a,\iota} \leq |\mathcal{A}| \cdot \nu_\iota \qquad \forall \iota \in \mathcal{I}, \tag{26a}$$

$$\nu_\iota \leq \sum_{a\in\mathcal{A}} \xi_{a,\iota} \qquad \forall \iota \in \mathcal{I}, \tag{26b}$$

$$\sum_{\iota\in\mathcal{I}} \nu_\iota \leq \mathfrak{N}. \tag{26c}$$

Here, $\mathfrak{N}$ denotes the user-defined maximum number of conductor types permitted in the system. As the decoupled CSS setting does not rely on the assumption that the array system forms a tree, the exact number of active edges in the system is unknown, particularly in the case of looped arrays. For this reason, constraint Eq. (26) allows greater flexibility in the selection of conductor types.

5 Joint routing and conductor size optimisation

In Section 4, conductor size selection was formulated assuming that the routing of the array system was already determined. Under this formulation, cable diameters are assigned to a fixed network topology. However, the routing configuration and conductor sizing are inherently coupled, since limiting the set of conductor types also limits the maximum transferable power within the network. Importantly, this limit is determined not by the largest conductor type available overall, but by the largest conductor type selected for use in the network.

To account for this interaction, conductor size selection can be coupled with the routing formulation. This allows routing decisions and conductor assignments to be evaluated within a coordinated optimisation framework. Two strategies are considered: an integrated formulation (Section 5.1) and a sequential algorithm (Section 5.2).

5.1 Integrated conductor size selection

In the integrated formulation, conductor size selection is incorporated directly into the routing optimisation. Each candidate edge may therefore be associated with multiple conductor types, and the optimisation determines both whether the edge is activated and which conductor type is assigned.

Each conductor type $\iota \in \mathcal{I}$ is characterised by a flow capacity $\mathfrak{M}_\iota$. To represent the assignment of conductor types to candidate edges, the binary edge activation variable is extended with an additional dimension $\xi_{a,\iota}$ associated with each branch. This variable links the activation of an edge to the selection of a specific cable type, such that

$$\sum_{\iota\in\mathcal{I}} \xi_{a,\iota} = \xi_a \qquad \forall a \in \mathcal{E}, \tag{27}$$

Here, the sum of assigned conductor types equals one if the branch is active and zero otherwise. As the flow limit now depends on the selected conductor type, Eq. (5) is modified to reflect type-specific capacities:

$$-\sum_{\iota\in\mathcal{I}}(\xi_{a,\iota}\cdot\mathfrak{M}_\iota)\leq f_a\leq\sum_{\iota\in\mathcal{I}}(\xi_{a,\iota}\cdot\mathfrak{M}_\iota)\,. \tag{28}$$

In this formulation, the parameter $\mathfrak{M}$ used in Eq. (7) is defined as the maximum value over all conductor capacities, i.e. $\mathfrak{M}=\max_{\iota\in\mathcal{I}}\mathfrak{M}_\iota$, ensuring that each branch satisfies criterion C3.To constrain the permissible number of active conductor types from the set and comply with criterion C5,the previously defined binary variable ν_ι is employed. Leveraging Eq. (3), which defines the total number of active branches based on the number of turbines and substations, the term $(|\mathcal{N}_t|)$ provides an upper bound on the number of branches. Accordingly, Eq. (26a) is reformulated as follows:

$$\sum_{a\in\mathcal{E}}\xi_{a,\iota}-|\mathcal{N}_t|\cdot\nu_\iota\leq 0\qquad\forall\iota\in\mathcal{I}. \tag{29}$$

The objective of the optimisation is to minimise the total cost of all active edges as follows:

$$\min\left[\sum_{a\in\mathcal{E}}\left(\xi_a\cdot\mathcal{W}_a\cdot\psi_a+\sum_{\iota\in\mathcal{I}}[\xi_{a,\iota}\cdot L_a\cdot\psi_\iota]\right)\right]. \tag{30}$$

Here, ψ_ι and ψ_a represent the cost per unit length of each cable type and the installation cost per unit of length, respectively. It is important to note that installation costs are based on the weighted length $\mathcal{W}_a$, which accounts for soft exclusions from graph preparation (d,e), while conductor costs are based on the actual length L_a of each segment. The objective thus captures a combined cost of installation and cable type selection.

However, the inclusion of cable size selection is mutually exclusive with the iterative determination of substation connections, as the computation of the initial connection set-point to the substation depends on the largest conductor used. If this is decided in advance, it constrains the space of possible solutions.

5.2 Sequential algorithm

To address this limitation, a sequential approach is proposed. This formulation allows the routing stage to incorporate more detailed constraints that would otherwise overly restrict the integrated optimisation problem. However, it also highlights a limitation of single-pass routing approaches. When routing is performed independently of CSS, the routing stage primarily minimises geometric length, while conductor costs are determined subsequently during cable size selection. As conductor capacity and cost do not scale linearly with diameter, the shortest trench or cable layout does not necessarily correspond to the minimum total investment cost.

This mismatch is further influenced by the definition of the maximum number of turbines per string, $\mathfrak{M}$, which is based on the capacity of the largest available conductor. Consequently, routing solutions that minimise cable length tend to favour configurations with a larger number of turbines per feeder, implicitly encouraging the use of higher-capacity cables and potentially increasing the overall investment cost.

The sequential algorithm, illustrated in Fig. 3, addresses this issue by iterating between routing and conductor sizing decisions. The procedure begins with the graph prepared using the method described in section 2 and considers a set of possible conductor types $\mathcal{I}$. In the first iteration, the minimum path connection problem (section 3) is solved in conjunction with the substation connection strategy described in subsubsection 3.2.2 to determine the trenching investment cost, denoted by Ψ_{MP}. The resulting subset of edges determined by the routing optimisation, $\mathcal{A}$, is then evaluated using either a non-linear CSS approach (subsection 4.1), which accounts for conductor losses and investment, or a linear CSS model (subsection 4.2), which focuses solely on conductor investment and is computationally more efficient.

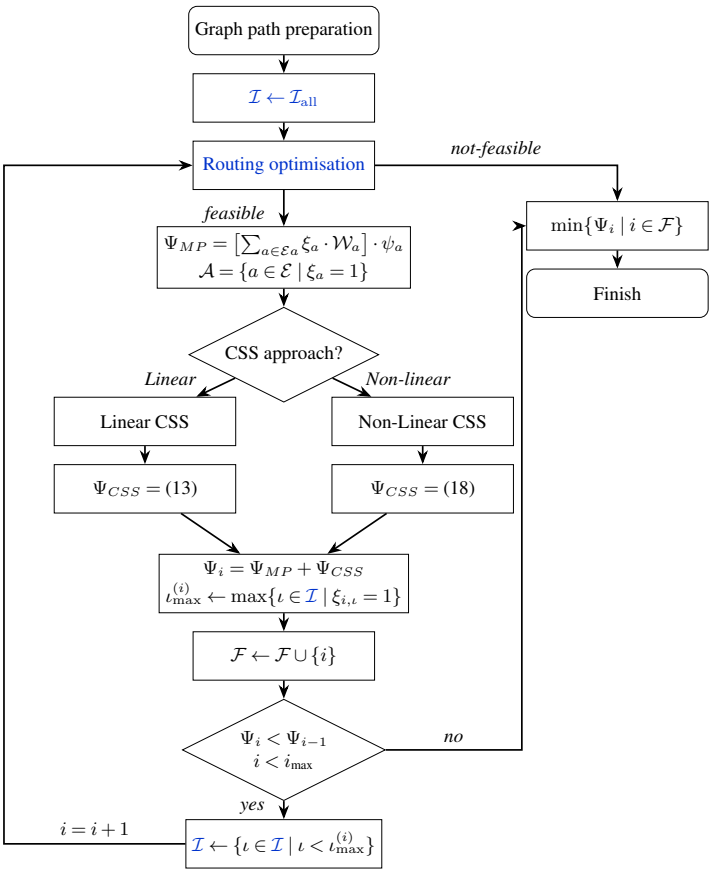

Figure 3. Sequential Algorithm

Following the CSS assignment, the total cost Ψ_i for iteration i is calculated by summing the trenching and conductor investment costs. The largest conductor type used in that iteration, denoted $\iota_{\max}^{(i)}$, is then identified. The solution is subsequently added to the feasible solution set $\mathcal{F}$.

In the subsequent iteration, the candidate conductor set $\mathcal{I}$ is restricted to conductor types with capacities strictly smaller than $\iota_{\max}^{(i)}$, and the procedure is repeated. This progressively limits the search to solutions relying on smaller conductor types. The algorithm terminates under three conditions: (i) if the routing problem becomes infeasible, for example due to path limitations,

a restricted number of allowable substation connections, or an empty conductor set; or (ii) if the user-defined iteration limit is reached, or (iii) if the reduction in conductor costs achieved by using smaller cable types is outweighed by the increase in trenching costs due to longer routing distances, resulting in a higher total cost than in the previous iteration.

The final array layout is selected as the solution with the minimum total cost from the feasible solution set $\mathcal{F}$.

6 Case studies

In this section, case studies are presented to illustrate the methodology. First, a set of case studies focuses solely on the layout MILP model and demonstrates how its adaptations result in different layouts. Second, offshore and onshore case studies are used to compare the multi-stage methodology when adopting either an integrated or a sequential approach. Finally, two wind parks are utilised to compare the use of linear and non-linear CSS within the sequential framework. The case studies presented in this paper are based on existing offshore and onshore wind parks in order to demonstrate the scope of the formulation. However, they cannot be directly compared with real projects, as the authors do not have access to internal cost data or to the specific technical details of the cables used in these developments. The data associated with the case studies, including array voltage, turbine rated power, and graph creation results from Section 2, such as the number of nodes, edges, crossings, and graph generation time, is presented in B, while the conductor type data is presented in C.

6.1 Layout modelling

To provide a visual example of the layout formulation and its refinements, the turbine distributions of *Baltic Eagle [DE]* and *Moray East [GB-SCT]* are used. Based on the turbine and substation locations, several tests are conducted. The different formulations evaluated correspond to the Type column in Table 1: the core formulation for determining minimum paths (Type 3.1); the inclusion of a constraint on the minimum number of turbines per string (Type 3.2.1); the refinement of the formulation to determine substation connections (Type 3.2.2); and the relaxation of constraint (6) to allow bifurcations (Type Relaxed (6)). For the case of *Baltic Eagle*, a hypothetical substation is additionally introduced and limited to a maximum of ten turbines to illustrate substations with different power limits (Type 3.2.3). The numerical results are reported in Table 1, while the corresponding layouts are shown in Fig. 4 for *Baltic Eagle [DE]* and in Fig. 5 for *Moray East [GB-SCT]*.

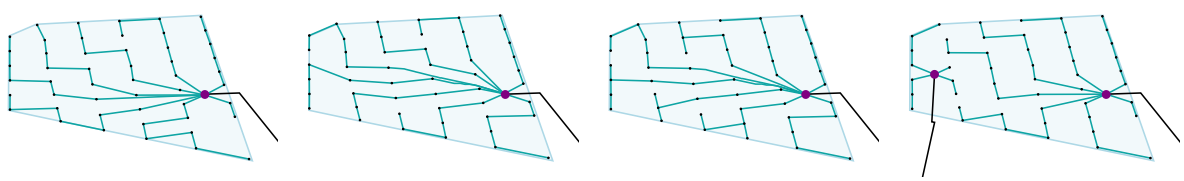

(a) (b) (c) (d)

Figure 4. *Baltic Eagle [DE]* array results: solutions from model parameters set to (a) Core formulation, (b) minimum number of turbines per string , (c) allowing bifurcations, and (d) irregular substation capacities.

Table 1. *Baltic Eagle [DE]* and *Moray East [GB-SCT]* minimum path finding solutions

Test system	Type	Visual result	Trench length [km]	Solution time [s]	$\mathfrak{S}_s$	$\mathfrak{m}$
Baltic Eagle [DE]	3.1	Fig. 4(a)	59.69	95.72	50	
	3.2.1	Fig. 4(b)	61.18	81.78	50	6
	3.2.2	Fig. 4(a)	59.69	40.52	8	
	3.2.1 & 3.2.2	Fig. 4(b)	61.18	74.78	8	6
	Relaxed (6)	Fig. 4(c)	56.31	203.59	8	6
	3.2.3	Fig. 4(d)	49.11	7.43	50	
Moray East [GB-SCT]	3.1	Fig. 5(a)	149.52	30.92	100	
	3.2.1				100	6
	3.2.2	Fig. 5(b)	151.44	102.40	5	
	3.2.1 & 3.2.2	Fig. 5(c)	152.04	141.65	6	5
	Relaxed (6)	Fig. 5(d)	149.08	235.83	6	5

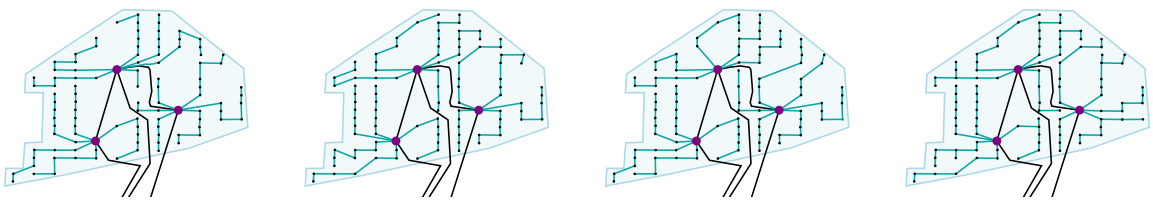

(a) (b) (c) (d)

Figure 5. *Moray East [GB-SCT]* array results: solutions from model parameters set to (a) Core formulation, (b) determining substation connections, (c) minimum number of turbines per string and determining substation connection , and (d) allowing bifurcations.

As shown in Fig. 4, the core formulation yields short strings that are balanced according to the minimum turbines-per-string constraint. However, for the *Moray East [GB-SCT]* case, the algorithm fails to produce a feasible solution under the minimum turbines-per-string criterion within the specified parameters, owing to limitations on inter-substation connectivity. In the subsequent formulation, where the minimum number of substation connections is determined iteratively, the solution time is reduced in both cases.

As illustrated in Table 1, relaxing the constraint (6) to allow radial-star configurations results in shorter trench lengths in both cases, although at higher computational cost. Since radial configurations are a subset of radial-star configurations, the resulting layouts cannot be shorter than those obtained with bifurcations; however, the reduced solution space can aid the solver in approaching optimality.

6.2 Test systems for joint optimisation

To enable broad application of the formulation, a cable database was created. For offshore cases, the database is based on copper cables from (ABB, 2010b) and includes 22 kV, 33 kV, and 66 kV voltage levels, covering ten conductor cross-sectional areas ranging from 95 mm^2 to 1000 mm^2. For onshore cases, the database is based on copper cables from (ABB, 2010a) at the 33 kV voltage level, covering fifteen cross-sectional areas from 95 mm^2 to 2000 mm^2, assuming buried cables under trefoil conditions.

In all simulations, the cost per metre of each conductor type is estimated using the procedure described in (Dicorato et al., 2011), which relates cost to the conductor's cross-sectional area. Based on the same reference, a trenching cost of 304 k€/km is used in offshore simulations. For onshore simulations, the trenching cost is assumed to be half this value, as no reliable public data were found.

In each case study, the number of conductor types is limited to $\mathfrak{N} = 3$, meaning that at most three conductor types from the cable database may be selected in the optimisation. In addition, no explicit general constraint is imposed on substation connections. Both the cable database and the implementation of the methodology are available in the repository (Valerio et al., 2025). Simulations were performed on a desktop computer equipped with a 12th Gen Intel® Core™ i5-12400 processor (2.50 GHz) and 64 GB of RAM. The *Gurobi* solver (Gurobi Optimization, LLC, 2024) was used to solve the mixed-integer linear problems.

For the integrated approach, a time limit of six hours (21,600 s) was imposed. In contrast, the sequential approach used a time limit of one and a half hours (5,400 s) per sub-problem; therefore, the total runtime may exceed this limit depending on the number of iterations required. In the sequential approach, all CSS evaluations are performed using the linear formulation presented in section 4.

To illustrate the joint routing and conductor optimisation, the case of *Westermost Rough [GB-ENG]* is first presented. This example uses the same graph shown in Fig. 1(f). For the sequential approach, the intermediate results of the algorithm iterations are depicted in Fig. 6(a)–Fig. 6(e).

In the first iteration, with all ten conductor capacities available, the minimum-route solution connects seven turbines per string, requiring a conductor size of 800 mm^2. In the second iteration, the 800 mm^2 and 1000 mm^2 conductors are excluded from the available options. The process continues until iteration five, where the total investment exceeds that of iteration four. The resulting optimal configuration includes cable types of 95, 120, and 185 mm^2.

For comparison, the integrated CSS result is shown in Fig. 6(f). This result uses the same conductor selection as iteration three of the sequential algorithm (see Fig. 6(c)). In iteration three, the connections to the substation are determined within the optimisation. In contrast, the integrated CSS does not perform this evaluation, allowing the algorithm to generate shorter strings, assign the 300 mm^2 conductor to only three strings, and increase the total number of strings, thereby reducing the overall cost. A detailed cost breakdown is provided in Table 2, where increases in cable length, trench length, and installation cost can be observed as the iterations progress; however, the total cost continues to decrease until the reduction in conductor costs no longer compensates for the additional trenching.

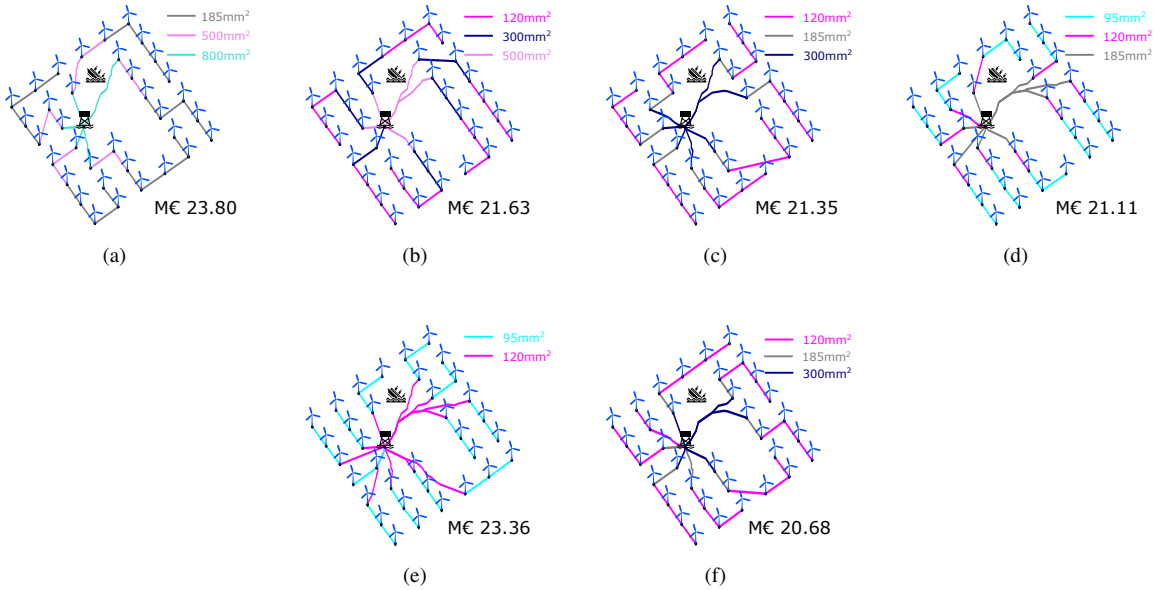

Figure 6. *Westermost Rough [GB-ENG]* array results: iterative solutions from (a) iteration 1 to (e) iteration 5, and (f) the integrated MILP formulation.

Table 2. *Westermost Rough [GB-ENG]* sequential compared to result of integrated approach array costs

Iteration	Conductors available [mm^2]	Cable length [km]	Conductor cost [M€]	Trench length [km]	Installation cost [M€]	Total cost [M€]
1	95, 120, 150, 185, 240, 300, 400, 500, 630, 800	40.75	11.84	39.40	11.98	23.81
2	95, 120, 150, 185, 240, 300, 400, 500, 630	41.45	9.44	40.08	12.19	21.62
3	95, 120, 150, 185, 240, 300, 400	44.20	8.32	42.85	13.03	21.34
4	95, 120, 150, 185, 240	46.26	7.58	44.90	13.65	21.23
5	95, 120, 150	52.19	7.89	50.83	15.45	23.34
Integrated	95, 120, 150, 185, 240, 300, 400, 500, 630, 800	43.10	7.92	41.95	12.75	20.67

Further case studies were implemented, covering wind parks ranging from 12 to 174 turbines, with power capacities between 2 and 14 MW, and including arrays with one to three substations. Detailed information of number of permissible edges, number of turbines, identified crossings, and turbine power and voltage is given in Table B1. The table also reports the graph preparation time for each case.

HornSea I [GB-ENG] (Fig. 7(a),7(b)) serves as the largest test case, with 174 turbines and three substations. *Anholt [DK]* (Fig. 7(c),Fig. 7(d)) highlights how inter-turbine edges are prevented from crossing export cables, in this case due to the connection from Anholt Island to Denmark. *Horn Rev 2 [DK]* (Fig. 7(e),7(f)) illustrates how the routing mechanism can identify non-direct string layouts to optimise interconnections. *Moray West [GB-SCT]* (Fig. 7(g),7(h)) exemplifies configurations with large-capacity turbines. *Seagreen [GB-SCT]* (Fig. 7(i),7(j)) demonstrates the use of irregular development areas, where densification of points generates non-standard edges that comply with spatial constraints.

Table 3 summarises all offshore test cases, reporting the objective value, solution time, and the final optimality gap if the time limit was reached. The optimality gap measures the difference between the best feasible solution and the solver's lower bound, which comes from LP relaxations and represents a provable bound on the optimal objective (Gurobi Optimization, LLC, 2024). Simulation times marked with an asterisk (*) indicate when the last feasible solution was obtained. Detailed results are given in Table D1 and Table D2 of the individual objective costs.

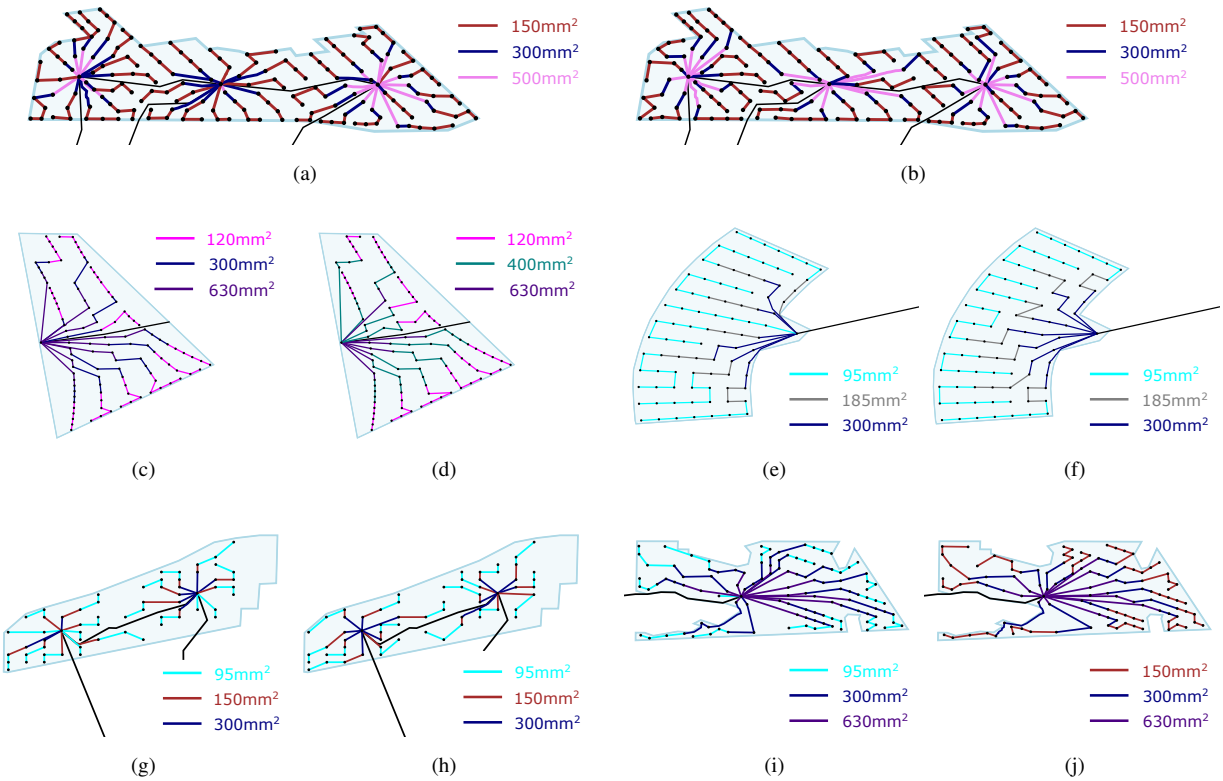

Figure 7. Offshore array results showing integrated and sequential CSS solutions respectively for each case: (a,b) *Hornsea I [GB-ENG]*, (c,d) *Anholt [DK]*, (e,f) *Horns Rev 2 [DK]*, (g,h) *Moray West [GB-SCT]*, (i,j) *Seagreen [GB-SCT]*

In the onshore cases, the z-plane incorporates elevation, with inclination playing a more significant role in further limiting the connectivity of the densified points. The test cases cover wind parks ranging from 10 to 106 turbines, with power capacities between 225 kW and 3.6 MW. Detailed information of number of permissible edges, number of turbines, identified crossings, and turbine power and voltage is given in Table B1.

For example, *Bhlaraidh [GB-SCT]* (Fig. 8(a),Fig. 8(b)) illustrates the role of exclusion zones in routing around water bodies such as lakes, while *Coromuel [MX]* (Fig. 8(c),Fig. 8(d)) demonstrates that the algorithm can still achieve feasible solutions in highly constrained development areas. Finally, Table 4 summarises all onshore test cases, reporting the objective value, solution time, and the final optimality gap if the time limit is reached. Simulation times marked with an asterisk (*) indicate

Table 3. Offshore wind test systems

Case	Figures	Integrated CSS			Sequential CSS		
		Cost [M €]	Time [s]	Gap [%]	Cost [M €]	Time [s]	Gap [%]
Albatros [DE]	–	9.62	2.88	0.00	9.72	5.04	0.00
Alpha ventus [DE]	–	4.17	0.95	0.00	4.17	1.81	0.00
Anholt [DK]	Fig. 7(c), 7(d)	72.74	3997.98*	4.40	73.29	6279.73	0.00
Arcadis Ost [DE]	–	15.65	8.71	0.00	16.11	9.80	0.00
Baltic eagle [DE]	–	28.83	64.87*	0.86	29.24	268.31	0.00
Barrow [GB-ENG]	–	7.82	5.26	0.00	7.85	8.58	0.00
Beatrice [GB-SCT]	–	68.42	122.42*	2.42	69.59	4342.30	0.01
DanTysk [DE]	–	48.93	14389.21*	2.32	49.55	177.54	0.00
Fryslaan [NL]	–	42.04	4592.39*	3.77	41.69	13156.39	0.50
Global Tech I [DE]	–	35.96	890.62*	2.30	35.72	1103.52	0.00
HornSea I [GB-ENG]	Fig. 7(a), 7(b)	173.01	3109.11*	1.86	177.76	16297.83	1.09
HornSea II [GB-ENG]	–	203.31	20185.3*	4.69	211.88	20372.22	3.22
HornsRev 1 [DK]	–	23.24	10656.14	0.01	23.37	72.11	0.01
HornsRev 2 [DK]	Fig. 7(e), 7(f)	30.73	224.68*	1.82	30.99	3306.68	0.00
HornsRev 3 [DK]	–	47.09	95.17	0.00	47.72	41.83	0.00
Kaskasi [DE]	–	15.90	357.43	0.00	16.41	56.15	0.00
Kentish [GB-ENG]	–	32.86	100.82*	0.64	33.15	16.90	0.00
Meerwind Sud Ost [DE]	–	33.60	96.00*	5.33	33.50	13405.85	1.19
Moray East [GB-SCT]	–	76.16	439.82*	0.69	76.51	284.13	0.00
Moray West [GB-SCT]	Fig. 7(g), 7(h)	54.88	53.35	0.00	56.54	63.65	0.00
Nordsee One [DE]	–	29.04	745.14	0.00	29.73	58.62	0.00
Nordsee Ost [DE]	–	20.26	36.26	0.00	20.73	34.20	0.00
Princess Amalia [NL]	–	15.98	70.80	0.00	15.75	43.24	0.00
Seagreen [GB-SCT]	Fig. 7(i), 7(j)	135.91	16777.35*	3.25	137.43	16244.64	1.08
Thanet [GB-ENG]	–	27.12	192.80*	0.70	27.41	5679.59	0.00
Triton Knoll [GB-ENG]	–	57.77	24.45*	1.17	59.07	438.52	0.00
West of Duddon [GB-ENG]	–	50.43	503.06*	5.29	50.03	27060.19	1.95
Westermost Rough [GB-ENG]	–	20.64	37.27	0.00	21.12	20.76	0.00

when the last feasible solution was obtained. The results in more details are given in Table D1 and Table D2 of the individual objective costs.

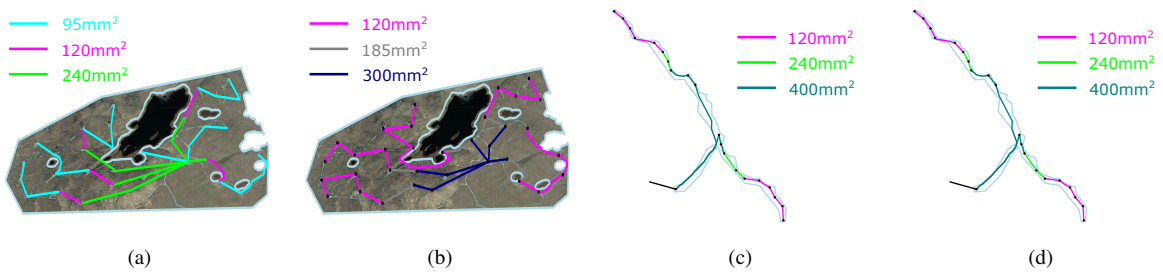

Figure 8. Onshore array results showing integrated and sequential CSS solutions respectively for each case: (a,b) *Bhlaraidh [GB-SCT]*, (c,d) *Coromuel [MX]*

Table 4. Onshore wind test systems

Case	Figures	Integrated CSS			Sequential CSS		
		Cost [M€]	Time [s]	Gap [%]	Cost [M€]	Time [s]	Gap [%]
Bhlaraidh [GB-SCT]	Fig. 8(a), 8(b)	5.68	24.76	0.00	6.28	37.11	0.00
Bronco Plains [US]	–	46.00	3052.73*	5.58	45.75	35675.22	0.00
Coromuel [MX]	Fig. 8(c), 8(d)	7.14	7.84	0.00	7.14	6.82	0.00
Griffin [GB-SCT]	–	14.58	20878.62*	6.14	14.68	9360.14	0.00
Serra Voltorera [ES]	–	0.55	1.17	0.00	0.94	1.71	0.00
Storheia vindpark [NO]	–	24.20	131.89*	5.76	24.64	28236.63	6.36
Stronelairg [NO]	–	14.33	4107.02	1.52	14.56	148.30	0.00
Trucafort one [ES]	–	1.65	8.08	0.00	1.70	12.84	0.00
Trucafort two [ES]	–	0.63	1.98	0.00	0.73	4.46	0.00

6.3 Comparison with Non-linear CSS approach

To bridge the difference to comparable project data, the inter-array documentation for *Moray East [GB-SCT]* (Marine Scotland, 2019) and *Moray West [GB-SCT]* (Marine Scotland, 2020) are used as a reference. In the simulations, cable selection is restricted to two aluminium types, with a maximum of eight and six strings per substation for *Moray East [GB-SCT]* and *Moray West [GB-SCT]*, respectively.

The simulation utilises four aluminium conductors, defined based on the cable capacities reported in (Marine Scotland, 2019, 2020) for conductor sizes of 240 mm^2, 300 mm^2, 650 mm^2, and 800 mm^2, as well as technical data and cost approximations from (ABB, 2010b; Dicorato et al., 2011). The project documentation specifies the cable length used for each conductor size, and for comparability, costs are calculated based on the same costs per length as those used in the simulations. The reported layout for *Moray East [GB-SCT]* is reproduced in Fig. 9(a) for comparison with Fig. 9(b), Fig. 9(c), and Fig. 9(d), while the reported layout for *Moray West [GB-SCT]* is presented in Fig. 9(e) and compared with Fig. 9(f), Fig. 9(g) and Fig. 9(h) which show the resulting layouts from the integrated and sequential methodologies, which show the simulation of integrated approach, linear sequential and non linear sequential approach respectively.

To account for losses, a non-linear approach is applied. Assuming an LCoE of 91 €/MWh and 5,170 full load hours annually over a 25-year project lifetime (Kost et al., 2024), a net present value analysis of losses relative to investment is conducted. To enable a direct comparison between losses and investment costs, the value of α in (18) is set to 1. For the non-linear simulation, the sequential algorithm is executed in a WSL environment, using OR-Tools (Perron and Furnon, 2025) for routing and Bonmin (Bonami et al., 2008) for the CSS.

In both cases, the non-linear CSS shown in Fig. 9(d) and Fig. 9(h) differs in conductor size selection from the linear solutions, while more closely resembling the reported project data. Comparing the linear and non-linear CSS for *Moray East*, the use of smaller conductor capacities is reduced, whereas higher-capacity conductors are utilised across a greater number of connections. In the case of *Moray West*, two strings connect six turbines instead of five, requiring a higher-capacity cable.

For a comparable assessment, losses are also calculated using a Newton–Raphson power flow applied to the grids obtained from the linear approaches. These results are presented in Table 5.

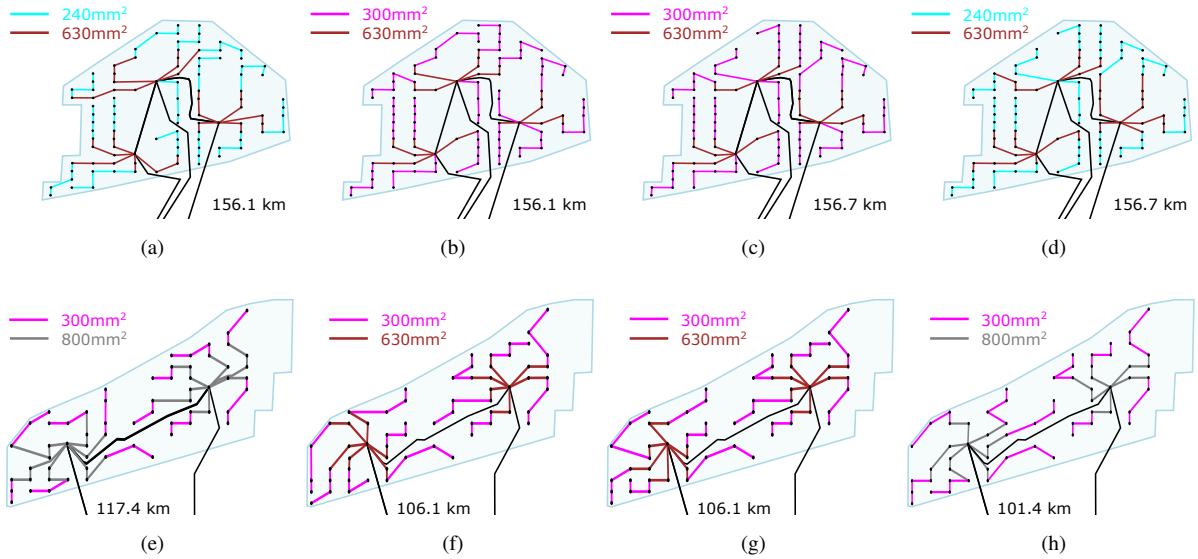

Figure 9. Project comparison for *Moray East* (a–d) and *Moray West* (e–h) [GB-SCT]: actual reported layouts and layouts obtained using the integrated, linear sequential, and non-linear sequential methodologies.

Table 5. *Moray East and West [GB-SCT]* projects

Case	Method	Figure	Length [km]	Costs [M€]				Time [s]
				Trench	Cable	Losses	Total	
Moray East [GB-SCT]	Reported layout Marine Scotland (2019)	Fig. 9(a)	156.100	46.094	48.059	32.657	126.810	–
	Integrated	Fig. 9(b)	156.064	44.595	45.839	34.582	125.016	3805.48*
	Linear sequential	Fig. 9(c)	156.735	44.797	45.823	34.730	125.350	54.661
	Non-linear sequential	Fig. 9(d)	156.735	44.797	46.455	28.267	119.519	19718.146
Moray West [GB-SCT]	Reported layout Marine Scotland (2020)	Fig. 9(e)	117.400	31.359	41.481	19.486	92.325	–
	Integrated	Fig. 9(f)	106.098	30.678	32.736	24.177	87.592	1105.498
	Linear sequential	Fig. 9(g)	106.093	30.677	32.888	25.222	88.786	34.757
	Non-linear sequential	Fig. 9(h)	106.093	29.241	36.037	23.331	86.508	1415.191

7 Discussion

The test systems presented above demonstrate the application of the graph preparation methodology, followed either by an integrated formulation of a mixed-integer linear programming model to address the routing task and conductor size selection, or by a sequential methodology that treats both problems separately. The iterative algorithm is designed to balance the allocation of turbines within strings and the distribution of strings across multiple substations. Where feasible, the algorithm favours

equal string sizes. When this is not possible due to buildable-area constraints, the optimisation starts from the closest feasible configuration.

The routing algorithm presents a core formulation that can be adapted to user requirements, as illustrated in Section 3.2, with potential for broader application. In the examples provided, the turbine layouts of *Baltic Eagle [DE]* and *Moray East [GB-SCT]* are used to illustrate comparisons across various optimisation objectives, including minimising the number of turbines per string, reducing the number of strings per substation, comparing configurations with radial-star layouts, and incorporating substations with limited power capacities. A detailed benchmarking of the routing formulation against the work of Souza de Alencar et al. (2025) is presented in Valerio et al. (2026b).

Shifting focus to full-park optimisation with CSS, as presented in Section 6.2, the integrated results reveal that in most cases the optimisation reaches the imposed time limit. However, feasible solutions are typically identified within a relatively short time window, after which the optimisation primarily focuses on reducing the optimality gap. Although the gap generally decreases over time, convergence can be slow, making it difficult to prove optimality within practical computational limits. Consequently, selecting an appropriate cut-off time that balances computational effort and solution quality remains non-trivial. For example, in the case of *Griffin [GB-SCT]*, the last feasible solution is found very close to the time limit.

By contrast, when using the sequential solution, even simple layouts tend to result in longer computation times, as the routing algorithm is executed repeatedly. In more complex layouts, the time limit is still often reached; however, because the underlying optimisation problem is simpler, the optimality gap is generally closed more efficiently. In Table 3 and Table 4, the gap presented in the sequential CSS column refers to the optimality gap of the resulting iteration of the routing algorithm, which in all cases is smaller than that of the integrated approach, or is zero.

The case studies presented above illustrate the application of the strategies to both offshore and onshore systems. In these cases, the algorithm determines the optimal combination of conductor sizes and pathways to interconnect all turbines. The algorithm achieved this under 5 seconds for the smaller systems. However, for the larger and more complex cases, the routing algorithm reached the predefined time limit. In such instances, while the solution is feasible, optimality cannot be guaranteed.

The problem is solved using the *Gurobi* solver, which applies a branch-and-bound algorithm to identify feasible solutions. Through the use of callbacks, the solver records both the objective value and the time at which each feasible solution is found. Solver progress for the Hornsea I test cases is illustrated in Fig. 10(a) for the integrated formulation, and in Fig. 10(b) and Fig. 10(c) for the sequential iterations of the routing and CSS stages, respectively.

Both Fig. 10(a) and Fig. 10(b) show rapid initial convergence, as reflected by the reduction in the optimality gap. The plots report the optimality gap at the moment each feasible solution is found. As the solver progresses, the lower bound may improve, meaning that the gap associated with earlier solutions would decrease if evaluated against the final bound. In Fig. 10(c), the solver reaches optimality quickly, indicating that the CSS stage is not restrictive in terms of solution time. Consequently, the routing stage becomes the primary determinant of overall optimality, and simplifying this stage through sequential iterations proves beneficial.

In all cases, the routing algorithm is constrained by the graph preparation process. Connections that may appear feasible upon visual inspection can be excluded due to cable crossing constraints, an inherent limitation of using static constraints. As

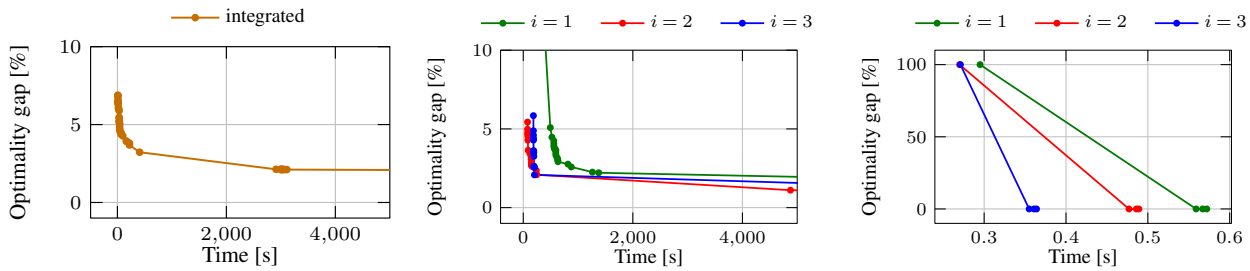

Figure 10. Solver progress for the case *HornSea I [GB-ENG]*: (a) Integrated CSS-MILP, (b) Sequential: minimum path connection with minimum turbines and determining substation connections and (c)Sequential: CSS

illustrated in Fig. 11(a), a visually preferable layout might involve connecting the leftmost turbine (highlighted in blue) of the orange string, directly to the substation, thereby reducing total cable length. However, this configuration is excluded by the algorithm because it intersects with other inter-turbine edges.

In another example, shown in Fig. 11(c), the connection set in orange originates from the original project documentation but would be excluded under the current method, as it crosses other active connections. Another restriction concerns the connectivity of possible turbine-to-turbine links. In the methodology proposed in Section 2, such connections are defined using Delaunay and diagonal edges. In Fig. 11(b), the orange link, also derived from the project documentation, would not be considered under a Delaunay-diagonal configuration. This could be extended, optionally, by incorporating k-nearest neighbours into the search; however, doing so increases the graph preparation time and complicates the routing problem.

Moreover, under the graph preparation procedure, connections originating from the substation and overlapping with other substation links are not classified as crossings by the algorithm. Consequently, multiple such connections are permitted. This is also visible in Fig. 11(a), where area constraints result in parallel segments running from the substation to different turbines. This examples underscores the importance not only of careful graph preparation but also of incorporating human oversight to mitigate limitations inherent in automated layout strategies.

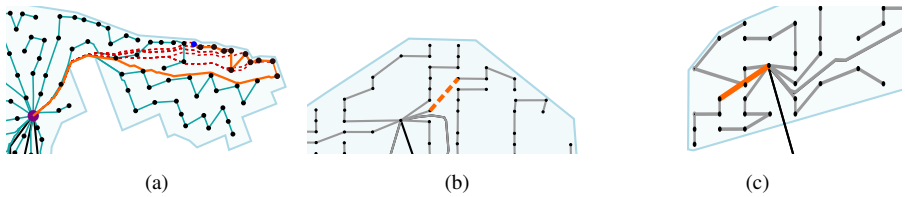

Figure 11. Onshore array results showing integrated and sequential CSS solutions respectively for each case: (a) Section of Hornsea II connectivity, (b) Moray East Delaunay and diagonals restriction, (c) Moray West Static Crossings

8 Conclusions

This paper presents a set of stages for the optimisation of inter-array grids in wind parks. Each stage may be applied independently to enhance existing workflows or combined into either an integrated or sequential algorithm, both of which are also introduced in this work. The first stage configures the graph representation of turbine and substation interconnections, taking into account bathymetry or elevation, inclination thresholds, export cables, and both soft and hard exclusion zones. The second stage introduces a core model to optimise a radial array, constraining bifurcations, crossings, and the number of turbines per string through the formulation of a mixed-integer problem. This model can be extended to accommodate a minimum number of turbines per string, determine the minimum number of substation connections required, or incorporate substations with different power capacities. The third stage addresses conductor size selection, limiting the number of selected conductors by employing a DC linear approximation of the power flow.

The second and third stages may be iterated within an integrated algorithm to solve the problem simultaneously or within a sequential algorithm to identify the optimal trade-off between the maximum number of turbines per string and conductor investment. These two approaches are compared across more than thirty case studies, in which the sequential approach further restricts the problem to enable the generation of layouts that are both technically feasible and electrically balanced.

The case studies are based on existing turbine ratings and locations, encompassing both onshore and offshore scenarios. While they demonstrate the strategies' usability, they cannot be directly compared to real project deployments, as the input data used by the authors differ from those of the individual projects. In the case of the Moray developments, where a realistic representation of cable paths was publicly available, the optimisation predicted a very similar interconnection layout.

Although the use of mixed-integer linear programming for joint routing and conductor sizing, either in an integrated formulation or in a sequential approach with linear or non-linear CSS, increases computational complexity relative to greedy heuristics, it provides a structured framework capable of addressing increasingly complex constraints encountered in real-world wind farm developments that are often overlooked in simpler models. However, the quality of the final layout remains sensitive to the granularity and accuracy of the graph preparation stage. As such, the approach is conceived as a planning support tool that aids the human design process, particularly in navigating complex physical and operational constraints.

Appendix A: List of symbols

A1 Sets and indices

$\mathcal{N}_{ac}$	Set of all nodes in the network
$\mathcal{N}_t$	Set of turbine nodes
$\mathcal{N}_s$	Set of substation nodes
$\mathcal{E}$	Set of candidate edges
$\mathcal{E}_i$	Set of edges connected to node i
$\mathcal{A}$	Set of active edges selected by the routing stage

$\mathcal{I}$	Set of available conductor types
i, k	Indices of network nodes
$a = (i, k)$	Edge connecting nodes i and k
ι	Index of conductor type
$\mathcal{F}$	Feasible solution set

A2 Decision variables

ξ_a	Binary variable indicating whether edge a is active
$\xi_{a,\iota}$	Binary variable indicating assignment of conductor type ι to edge a
ν_ι	Binary variable indicating whether conductor type ι is used
f_a	Integer power flow on edge a
$z_{a,\iota}$	Auxiliary variable for McCormick linearisation
$\iota_{\max}^{(i)}$	Largest conductor type that was assigned

A3 Routing design parameters

p_i	Net power injection at node i
$\mathfrak{M}$	Maximum number of turbines per string
$\mathfrak{m}$	Minimum number of turbines per string
$\mathfrak{s}_s$	Minimum number of string connections per substation
$\mathfrak{S}_s$	Maximum number of connections per substation
$\mathfrak{M}_\iota$	Flow capacity of conductor type ι
$\mathfrak{N}$	Maximum number of conductor types allowed
$\mathcal{W}_a$	Weighted length of edge a
L_a	Geometric length of edge a
ψ_a	Installation cost per unit weighted length
ψ_ι	Cost per unit length of conductor type ι

A4 Electrical quantities

V_i	Voltage magnitude at node i
θ_i	Voltage angle at node i
P_{ik}, Q_{ik}	Active and reactive power flow from node i to node k
S_{ik}	Apparent power flow from node i to node k

$S_{a,\iota_{ik}}$	Apparent power flow on branch a using conductor type ι
P_{t_i}, Q_{t_i}	Active and reactive turbine power at node i
P_{s_i}, Q_{s_i}	Active and reactive substation power at node i
γ_{t_i}	Curtailment factor at turbine node i
M_a	Big-M parameter for branch a
κ	Security factor for M_a

A5 Economic parameters

α	Weighting parameter in the multi-objective function
r	Discount rate
y	Project lifetime (years)
H_y	Full-load hours over y years
ρ	Electricity cost

Appendix B: Case Information

This appendix provides detailed information on the test cases and their corresponding results. Table B1 summarises the specific characteristics of each case.

Appendix C: Conductor dataset

This appendix provides information on the conductor sets used in the test cases. The cable data are compiled from (ABB, 2010a) for onshore cables and (ABB, 2010b) for offshore submarine cables. In all simulations, the cost per metre of each conductor is estimated as

$$\text{Cost} = 0.4818 \cdot S + 99.153 \quad [\text{k€ km}^{-1}], \tag{C1}$$

taken from Dicorato et al. (2011), where S denotes the conductor cross-sectional area. In this approximation, neither the voltage level nor the conductor material is explicitly considered. Consequently, the resulting cost values are employed solely for methodology validation within the presented case studies and should not be interpreted as industrial quotations, project-specific estimates, or commercially validated cable prices.

For onshore 33 kV cables in Table C1, reference (ABB, 2010a) does not provide data directly; therefore, the corresponding values were extrapolated from the available voltage levels. For the conductors used in the Non-linear CSS in Table C6, the cable parameters are taken from the ABB dataset, whereas the cable capacities are taken from (Marine Scotland, 2019, 2020).

Table B1. Cases detailed information

Case	Turbine	Array	Graph			
	Power [MW]	Voltage [kV]	Nodes	Edges	Crossings	Time [s]
Albatros [DE]	7	33	17	67	150	3.08
Alpha ventus [DE]	5	66	13	48	93	1.37
Anholt [DK]	3.6	33	112	514	1853	25.32
Arcadis Ost [DE]	9.5	66	28	120	357	8.61
Baltic eagle [DE]	9.5	66	51	270	1113	8.93
Barrow [GB-ENG]	3	33	31	150	643	5.87
Beatrice [GB-SCT]	7	33	86	506	5111	28.66
DanTysk [DE]	3.6	33	81	386	2152	20.74
Fryslaan [NL]	4.3	33	90	528	2964	17.14
Global Tech I [DE]	5	33	81	443	1764	16.66
HornSea I [GB-ENG]	7	33	177	1144	32700	115.54
HornSea II [GB-ENG]	8	66	166	859	4869	46.87
HornsRev 1 [DK]	2	33	81	470	2469	15.68
HornsRev 2 [DK]	2.3	33	92	488	2440	15.06
HornsRev 3 [DK]	8	33	50	254	770	10.12
Kaskasi [DE]	8	66	39	184	666	5.14
Kentish [GB-ENG]	3	33	44	230	905	7.98
Meerwind Sud Ost [DE]	3.6	33	81	418	1818	12.77
Moray East [GB-SCT]	9.5	66	103	619	13429	47.19
Moray West [GB-SCT]	14	66	62	330	2523	20.66
Nordsee One [DE]	6.2	33	55	274	1022	9.65
Nordsee Ost [DE]	6.2	66	43	205	576	7.28
Princess amalia [NL]	2	22	61	328	1124	9.70
Seagreen [GB-SCT]	10	66	115	634	3213	28.39
Thanet [GB-ENG]	3	33	101	571	2803	16.07
Triton Knoll [GB-ENG]	9.5	66	92	515	6257	21.92
West of Duddon [GB-ENG]	3.6	33	109	599	2627	17.77
Westermost Rough [GB-ENG]	6	33	36	154	410	9.55
Bhlaraidh [GB-SCT]	3.45	33	34	167	693	15.69
Bronco Plains [US]	2.8	33	107	617	3079	20.06
Coromuel [MX]	2.8	33	21	55	190	8.86
Griffin [GB-SCT]	2.3	33	69	336	2275	12.80
Serra Voltorera [ES]	1.67	33	11	38	256	1.27
Storheia vindpark [NO]	3.6	33	81	428	3203	48.71
Stronelairg [NO]	3.45	33	64	504	1115	16.75
Trucafort one [ES]	0.225	33	66	313	2649	8.58
Trucafort two [ES]	0.6	33	26	88	306	3.04

Table C1. ABB XLPE Cu 33 kV ground trefoil cable parameters

Cross-sectional area(S) [mm^2]	Capacitance [μF km^{-1}]	Power capacity [MVA]	Cost [€ km^{-1}]
95	0.191	13.146	144,924
120	0.196	14.932	156,969
150	0.224	16.719	171,423
185	0.234	18.862	188,286
240	0.258	22.006	214,785
300	0.278	24.721	243,693
400	0.313	28.364	291,873
500	0.347	32.223	340,053
630	0.377	36.581	402,687
800	0.407	41.225	484,593
1000	0.452	45.583	580,953
1200	0.517	48.941	677,313
1400	0.551	51.871	773,673
1600	0.581	54.228	870,033
2000	0.626	58.301	1,062,753

Table C2. ABB XLPE Cu 66 kV ground trefoil cable parameters

Cross-sectional area(S) [mm^2]	Capacitance [μF km^{-1}]	Power capacity [MVA]	Cost [€ km^{-1}]
95	0.160	26.293	144,924
120	0.180	29.865	156,969
150	0.190	33.437	171,423
185	0.200	37.724	188,286
240	0.220	44.011	214,785
300	0.240	49.441	243,693
400	0.260	56.729	291,873
500	0.290	64.445	340,053
630	0.320	73.162	402,687
800	0.350	82.450	484,593
1000	0.380	91.166	580,953
1200	0.430	97.883	677,313
1400	0.460	103.741	773,673
1600	0.490	108.457	870,033
2000	0.520	116.602	1,062,753

Table C3. ABB XLPE Cu 20 kV submarine cable parameters

Cross-sectional area(S) [mm^2]	Capacitance [μF km^{-1}]	Power capacity [MVA]	Cost [€ km^{-1}]
95	0.230	10.392	144,924
120	0.250	11.778	156,969
150	0.270	12.990	171,423
185	0.290	14.549	188,286
240	0.320	16.628	214,785
300	0.350	18.360	243,693
400	0.390	20.438	291,873
500	0.430	22.690	340,053
630	0.480	24.768	402,687

Table C4. ABB XLPE Cu 33 kV submarine cable parameters

Cross-sectional area(S) [mm^2]	Capacitance [μF km^{-1}]	Power capacity [MVA]	Cost [€ km^{-1}]
95	0.180	17.147	144,924
120	0.190	19.434	156,969
150	0.210	21.434	171,423
185	0.220	24.006	188,286
240	0.240	27.436	214,785
300	0.260	30.294	243,693
400	0.290	33.723	291,873
500	0.320	37.438	340,053
630	0.350	40.868	402,687
800	0.380	44.297	484,593

Table C5. ABB XLPE Cu 66 kV submarine cable parameters

Cross-sectional area(S) [mm^2]	Capacitance [μF km^{-1}]	Power capacity [MVA]	Cost [€ km^{-1}]
95	0.170	34.295	144,924
120	0.180	38.867	156,969
150	0.190	42.868	171,423
185	0.200	48.012	188,286
240	0.220	54.871	214,785
300	0.240	60.587	243,693
400	0.260	67.446	291,873
500	0.290	74.877	340,053
630	0.320	81.735	402,687
800	0.350	88.594	484,593
1000	0.380	94.310	580,953

Table C6. ABB XLPE Al 66 kV submarine cable parameters

Cross-sectional area(S) [mm^2]	Resistance [Ω km^{-1}]	Inductance [mH km^{-1}]	Capacitance [μF km^{-1}]	Power capacity [MVA]	Cost Cost [€ km^{-1}]
240	0.151	0.380	0.220	40.0	214,785
300	0.121	0.370	0.240	54.0	243,693
630	0.060	0.330	0.320	80.0	402,687
800	0.049	0.320	0.350	84.2	484,593

Appendix D: Detailed results

This annex provides detailed restuls on the test cases presented in subsection 6.2, Table D1 and Table D2 present the detailed outcomes for the integrated and sequential CSS methodologies, respectively.

Table D1. Integrated CSS wind test systems detailed results

Case	Cable length [km]	Conductor cost [M€]	Trench weighted length [km]	Installation cost [M€]	Total cost [M€]
Albatros [DE]	19.17	4.18	17.89	5.44	3.08
Alpha ventus [DE]	9.74	1.41	9.08	2.76	1.37
Anholt [DK]	127.84	34.94	124.32	37.79	25.32
Arcadis Ost [DE]	33.58	6.18	31.16	9.47	8.61
Baltic Eagle [DE]	60.05	11.91	55.66	16.92	8.93
Barrow [GB-ENG]	17.32	2.85	16.37	4.98	5.87
Beatrice [GB-SCT]	120.93	33.96	113.38	34.47	28.66
DanTysk [DE]	93.96	21.58	89.95	27.35	20.74
Fryslaan [NL]	77.70	18.61	77.09	23.44	17.14
Global Tech I [DE]	73.36	15.55	67.14	20.41	16.66
HornSea I [GB-ENG]	336.42	73.86	326.14	99.15	115.54
HornSea II [GB-ENG]	363.74	96.21	352.30	107.10	46.87
HornsRev 1 [DK]	49.89	8.48	48.57	14.77	15.68
HornsRev 2 [DK]	64.96	11.62	62.87	19.11	15.06
HornsRev 3 [DK]	92.47	19.42	91.01	27.67	10.12
Kaskasi [DE]	33.64	6.21	31.88	9.69	5.14
Kentish [GB-ENG]	60.57	14.54	60.27	18.32	7.98
Meerwind Sud Ost [DE]	65.13	14.95	61.33	18.64	12.77
Moray East [GB-SCT]	162.33	29.66	152.95	46.50	47.19
Moray West [GB-SCT]	112.06	22.39	106.90	32.50	20.66
Nordsee One [DE]	56.46	12.78	53.47	16.26	9.65
Nordsee Ost [DE]	45.89	6.90	43.94	13.36	7.28
Princess amalia [NL]	36.06	5.80	33.47	10.17	9.70
Seagreen [GB-SCT]	243.99	65.36	232.09	70.56	28.39
Thanet [GB-ENG]	58.87	10.48	54.73	16.64	16.07
Triton Knoll [GB-ENG]	118.64	22.63	115.59	35.14	21.92
West of Duddon [GB-ENG]	102.05	20.71	97.76	29.72	17.77
Westermost Rough [GB-ENG]	43.26	7.91	41.89	12.74	9.55
Bhlaraidh [GB-SCT]	17.52	3.02	17.52	2.66	15.69
Bronco Plains [US]	112.40	28.91	112.40	17.08	20.06
Coromuel [MX]	18.13	4.38	18.13	2.76	8.86
Griffin [GB-SCT]	40.90	8.37	40.90	6.22	12.80
Serra Voltorera [ES]	1.85	0.27	1.85	0.28	1.27
Storheia vindpark [NO]	56.22	15.66	56.22	8.55	48.71
Stronelairg [NO]	46.39	8.56	46.39	7.05	16.75
Trucafort one [ES]	5.54	0.80	5.54	0.84	8.58
Trucafort two [ES]	2.13	0.31	2.13	0.32	3.04

Table D2. Sequential CSS wind test systems detailed results

Case	Cable length [km]	Conductor cost [M €]	Trench weighted length [km]	Installation cost [M €]	Total cost [M €]
Albatros [DE]	20.69	3.82	19.41	5.90	9.72
Alpha ventus [DE]	9.74	1.41	9.08	2.76	4.17
Anholt [DK]	129.47	35.00	125.96	38.29	73.29
Arcadis Ost [DE]	32.58	6.94	30.17	9.17	16.11
Baltic Eagle [DE]	63.37	11.31	58.98	17.93	29.24
Barrow [GB-ENG]	17.66	2.77	16.71	5.08	7.85
Beatrice [GB-SCT]	134.08	31.12	126.52	38.46	69.59
DanTysk [DE]	95.29	21.80	91.27	27.75	49.55
Fryslaan [NL]	74.01	19.38	73.40	22.31	41.69
Global Tech I [DE]	76.57	14.33	70.35	21.39	35.72
HornSea I [GB-ENG]	333.91	79.37	323.63	98.38	177.76
HornSea II [GB-ENG]	346.94	109.89	335.49	101.99	211.88
HornsRev 1 [DK]	49.88	8.61	48.56	14.76	23.37
HornsRev 2 [DK]	64.58	11.99	62.49	19.00	30.99
HornsRev 3 [DK]	94.24	19.52	92.77	28.20	47.72
Kaskasi [DE]	34.27	6.53	32.52	9.88	16.41
Kentish [GB-ENG]	60.54	14.84	60.24	18.31	33.15
Meerwind Sud Ost [DE]	64.50	15.05	60.70	18.45	33.50
Moray East [GB-SCT]	166.26	28.82	156.89	47.69	76.51
Moray West [GB-SCT]	112.86	20.16	107.69	32.74	52.90
Nordsee One [DE]	51.96	14.84	48.98	14.89	29.73
Nordsee Ost [DE]	46.69	7.13	44.75	13.60	20.73
Princess amalia [NL]	36.05	5.58	33.46	10.17	15.75
Seagreen [GB-SCT]	244.60	66.69	232.69	70.74	137.43
Thanet [GB-ENG]	59.04	10.72	54.90	16.69	27.41
Triton Knoll [GB-ENG]	124.65	22.10	121.61	36.97	59.07
West of Duddon [GB-ENG]	99.51	21.08	95.23	28.95	50.03
Westermost Rough [GB-ENG]	46.01	7.54	44.65	13.57	21.12
Bhlaraidh [GB-SCT]	18.77	3.43	18.77	2.85	6.28
Bronco Plains [US]	119.77	27.55	119.77	18.21	45.75
Coromuel [MX]	18.13	4.38	18.13	2.76	7.14
Griffin [GB-SCT]	40.22	8.56	40.22	6.11	14.68
Serra Voltorera [ES]	3.12	0.46	3.12	0.47	0.94
Storheia vindpark [NO]	55.05	16.28	55.05	8.37	24.64
Stronelairg [NO]	42.63	8.08	42.63	6.48	14.56
Trucafort one [ES]	5.74	0.83	5.74	0.87	1.70
Trucafort two [ES]	2.46	0.36	2.46	0.37	0.73

Code and data availability. Code for the optimisation is available as part of the *pyflow-acdc* v0.5.1 (Valerio et al., 2025) python package. The data and code to run all case studies is presented in Castro Valerio (2026).

Author contributions. Bernardo Castro Valerio:Writing– original draft & review and editing, Conceptualization, Data curation, Formal analysis, Methodology, Software, Validation, Visualization. Pieter Gebraad: Data curation, Writing review and editing, Funding acquisition, Supervision. Marc Cheah-Mane: Writing review and editing, Funding acquisition, Supervision. Vinicius Lacerda: Writing review and editing, Funding acquisition, Project administration, Supervision. Oriol Gomis-Bellmunt: Writing review and editing, Funding acquisition, Project administration, Supervision.

Competing interests. The authors declare that they have no conflict of interest.

Acknowledgements. This work has received funding from the ADOreD project of the European Union's Horizon Europe Research and Innovation program under the Marie Skłodowska-Curie grant agreement No 101073554.

During the preparation of this work the authors used GPT-4o in order to improve grammar and language readability. After using this tool/service, the authors reviewed and edited the content as needed and take full responsibility for the content of the publication.

References

ABB: XLPE Land Cable Systems: User's Guide, ABB, rev. 5 edn., 2010a.

ABB: XLPE Submarine Cable Systems: Attachment to XLPE Land Cable Systems - User's Guide, ABB, rev. 5 edn., https://new.abb.com/docs/default-source/ewea-doc/xlpe-submarine-cable-systems-2gm5007.pdf, 2010b.

BGV Associates: Wind Farm Costs, https://guidetoanoffshorewindfarm.com/wind-farm-costs/, 2025.

Bonami, P., Biegler, L. T., Conn, A. R., Cornuéjols, G., Grossmann, I. E., Laird, C. D., Lee, J., Lodi, A., Margot, F., Sawaya, N., and Wächter, A.: An algorithmic framework for convex mixed integer nonlinear programs, Discrete Optimization, 5, 186–204, https://doi.org/https://doi.org/10.1016/j.disopt.2006.10.011, in Memory of George B. Dantzig, 2008.

Castro Valerio, B.: Code and data for Case Studies of: A multi-stage methodology for wind park inter-array cabling: graph preparation, layout, and sizing, https://doi.org/10.5281/zenodo.18937430, 2026.

Cazzaro, D. and Pisinger, D.: Balanced cable routing for offshore wind farms with obstacles, Networks, 80, 386–406, https://doi.org/https://doi.org/10.1002/net.22100, 2022.

Cazzaro, D., Fischetti, M., and Fischetti, M.: Heuristic algorithms for the Wind Farm Cable Routing problem, Applied Energy, 278, 115 617, https://doi.org/10.1016/j.apenergy.2020.115617, 2020.

Chen, Y., Dong, Z. Y., Meng, K., Luo, F., Xu, Z., and Wong, K. P.: Collector System Layout Optimization Framework for Large-Scale Offshore Wind Farms, IEEE Transactions on Sustainable Energy, 7, 1398–1407, https://doi.org/10.1109/TSTE.2016.2549602, 2016.

Dicorato, M., Forte, G., Pisani, M., and Trovato, M.: Guidelines for assessment of investment cost for offshore wind generation, Renewable Energy, 36, 2043–2051, https://doi.org/10.1016/j.renene.2011.01.003, 2011.

Dutta, S. and Overbye, T. J.: Optimal Wind Farm Collector System Topology Design Considering Total Trenching Length, IEEE Transactions on Sustainable Energy, 3, 339–348, https://doi.org/10.1109/TSTE.2012.2185817, 2012.

El Mokhi, C. and Addaim, A.: Optimal Substation Location Of A Wind Farm Using Different Metaheuristic Algorithms, in: 2020 IEEE 6th International Conference on Optimization and Applications (ICOA), pp. 1–6, https://doi.org/10.1109/ICOA49421.2020.9094469, 2020.

Fischetti, M. and Pisinger, D.: Optimizing wind farm cable routing considering power losses, European Journal of Operational Research, 270, 917–930, https://doi.org/10.1016/j.ejor.2017.07.061, 2018a.

Fischetti, M. and Pisinger, D.: Optimal wind farm cable routing: Modeling branches and offshore transformer modules, Networks, 72, 42–59, https://doi.org/10.1002/net.21804, 2018b.

GEBCO Bathymetric Compilation Group: The GEBCO_2025 Grid – a continuous terrain model for oceans and land at 15 arc-second intervals, NERC EDS British Oceanographic Data Centre, NOC, https://doi.org/10.5285/37c52e96-24ea-67ce-e063-7086abc05f29, 2025.

Gong, X., Kuenzel, S., and Pal, B. C.: Optimal Wind Farm Cabling, IEEE Transactions on Sustainable Energy, 9, 1126–1136, https://doi.org/10.1109/TSTE.2017.2771147, 2018.

Gurobi Optimization, LLC: Gurobi Optimizer Reference Manual, https://www.gurobi.com, 2024.

Hagberg, A. A., Schult, D. A., and Swart, P. J.: Exploring Network Structure, Dynamics, and Function using NetworkX, Python in Science Conference, https://doi.org/10.25080/TCWV9851, 2008.

Hou, P., Hu, W., Chen, C., and Chen, Z.: Overall Optimization for Offshore Wind Farm Electrical System, Wind Energy, 20, https://doi.org/10.1002/we.2077, 2016.

Hou, P., Zhu, J., Ma, K., Yang, G., Hu, W., and Chen, Z.: A review of offshore wind farm layout optimization and electrical system design methods, Journal of Modern Power Systems and Clean Energy, 7, 975–986, https://doi.org/10.1007/s40565-019-0550-5, 2019.

Kallinger, M. D., Rapha, J. I., Trubat Casal, P., and Domínguez-García, J. L.: Offshore Electrical Grid Layout Optimization for Floating Wind—A Review, Clean Technologies, 5, 791–827, https://doi.org/10.3390/cleantechnol5030039, 2023.

Kost, C., Müller, P., Sepulveda Schweiger, J., Fluri, V., and Thomsen, J.: Levelized Cost of Electricity of Renewable Energy Technologies, Tech. rep., Fraunhofer Institute for Solar Energy Systems ISE, 2024.

Marine Scotland: Moray East Offshore Wind Farm Cable Plan, Tech. rep., Marine Scotland, https://marine.gov.scot/sites/default/files/owf_cable_plan_v2_final_redacted.pdf, 2019.

Marine Scotland: Moray West Offshore Wind Farm Cable Plan, Tech. rep., Marine Scotland, https://marine.gov.scot/sites/default/files/846005-dbha10-mww-pln-000001_moray_west_wind_farm_cable_plan_rev01.pdf, 2020.

Moon, W.-S., Kim, J.-C., Jo, A., and Won, J.-N.: Grid optimization for offshore wind farm layout and substation location, in: 2014 IEEE Conference and Expo Transportation Electrification Asia-Pacific (ITEC Asia-Pacific), pp. 1–6, https://doi.org/10.1109/ITEC-AP.2014.6941124, 2014.

Perron, L. and Furnon, V.: OR-Tools, https://developers.google.com/optimization/, 2025.

Pillai, A., Chick, J., Johanning, L., Khorasanchi, M., and de Laleu, V.: Offshore wind farm electrical cable layout optimization, Engineering Optimization, 47, 1689–1708, https://doi.org/10.1080/0305215X.2014.992892, 2015.

Pérez-Rúa, J.-A. and Cutululis, N. A.: Electrical Cable Optimization in Offshore Wind Farms—A Review, IEEE Access, 7, 85 796–85 811, https://doi.org/10.1109/ACCESS.2019.2925873, 2019.

Pérez-Rúa, J.-A., Stolpe, M., and Cutululis, N. A.: Integrated Global Optimization Model for Electrical Cables in Offshore Wind Farms, IEEE Transactions on Sustainable Energy, 11, 1965–1974, https://doi.org/10.1109/TSTE.2019.2948118, 2020.

Qi, Y., Hou, P., Yang, L., and Yang, G.: Simultaneous Optimisation of Cable Connection Schemes and Capacity for Offshore Wind Farms via a Modified Bat Algorithm, Applied Sciences, 9, 265, https://doi.org/10.3390/app9020265, 2019.

Rentschler, M. U., Adam, F., and Chainho, P.: Design optimization of dynamic inter-array cable systems for floating offshore wind turbines, Renewable and Sustainable Energy Reviews, 111, 622–635, https://doi.org/10.1016/j.rser.2019.05.024, 2019.

Sedighi, M., Moradzadeh, M., Kukrer, O., and Fahrioglu, M.: Simultaneous optimization of electrical interconnection configuration and cable sizing in offshore wind farms, Journal of Modern Power Systems and Clean Energy, 6, 749–762, https://doi.org/10.1007/s40565-017-0366-0, 2018.

Serrano González, J., Burgos Payán, M., Santos, J. M. R., and González-Longatt, F.: A review and recent developments in the optimal wind-turbine micro-siting problem, Renewable and Sustainable Energy Reviews, 30, 133–144, https://doi.org/https://doi.org/10.1016/j.rser.2013.09.027, 2014.

Smail, H., Alkama, R., and Medjdoub, A.: Optimal design of the electric connection of a wind farm, Energy, 165, 972–983, https://doi.org/10.1016/j.energy.2018.10.015, 2018.

Souza de Alencar, M., Göçmen, T., and Cutululis, N. A.: Flexible cable routing framework for wind farm collection system optimization, European Journal of Operational Research, https://doi.org/10.1016/j.ejor.2025.07.069, 2025.

Taylor, P., Yue, H., Campos-Gaona, D., Anaya-Lara, O., and Jia, C.: Wind farm array cable layout optimisation for complex offshore sites—A decomposition based heuristic approach, IET Renewable Power Generation, 17, 243–259, https://doi.org/https://doi.org/10.1049/rpg2.12593, 2023.

Ulku, I. and Alabas-Uslu, C.: Optimization of cable layout designs for large offshore wind farms, International Journal of Energy Research, 44, 6297–6312, https://doi.org/10.1002/er.5336, 2020.

Valerio, B. C., Lacerda, V. A., Cheah-Mane, M., Gebraad, P., and Gomis-Bellmunt, O.: An optimal power flow tool for AC/DC systems, applied to the analysis of the North Sea Grid for offshore wind integration, IEEE Transactions on Power Systems, pp. 1–14, https://doi.org/10.1109/TPWRS.2025.3533889, 2025.

Valerio, B. C., Cheah-Mane, M., Lacerda, V. A., Gebraad, P., and Gomis-Bellmunt, O.: Transmission expansion planning for hybrid AC/DC grids using a mixed-integer non-linear programming approach, International Journal of Electrical Power & Energy Systems, 174, 111 459, https://doi.org/https://doi.org/10.1016/j.ijepes.2025.111459, 2026a.

Valerio, B. C., Gebraad, P. M., Cheah-Mane, M., Lacerda, V., and Gomis-Bellmunt, O.: Strategies for wind park inter array optimisation through Mixed Integer Linear Programming, Journal of Physics: Conference Series, 3224, 052 005, https://doi.org/10.1088/1742-6596/3224/5/052005, 2026b.

Virtanen, P., Gommers, R., Oliphant, T. E., and et al.: SciPy 1.0: Fundamental Algorithms for Scientific Computing in Python, Nature Methods, 17, 261–272, https://doi.org/10.1038/s41592-019-0686-2, 2020.

Wei, S., Zhang, L., Xu, Y., Fu, Y., and Li, F.: Hierarchical Optimization for the Double-Sided Ring Structure of the Collector System Planning of Large Offshore Wind Farms, IEEE Transactions on Sustainable Energy, 8, 1029–1039, https://doi.org/10.1109/TSTE.2016.2646061, 2017.

Wędzik, A., Siewierski, T., and Szypowski, M.: A new method for simultaneous optimizing of wind farm's network layout and cable cross-sections by MILP optimization, Applied Energy, 182, 525–538, https://doi.org/10.1016/j.apenergy.2016.08.094, 2016.